



Kinetics of phase transformations in the peridynamic formulation of continuum mechanics

Kaushik Dayal, Kaushik Bhattacharya*

Division of Engineering, California Institute of Technology, Pasadena, CA 91125, USA

Received 25 November 2005; received in revised form 26 March 2006; accepted 1 April 2006

Abstract

We study the kinetics of phase transformations in solids using the peridynamic formulation of continuum mechanics. The peridynamic theory is a nonlocal formulation that does not involve spatial derivatives, and is a powerful tool to study defects such as cracks and interfaces.

We apply the peridynamic formulation to the motion of phase boundaries in one dimension. We show that unlike the classical continuum theory, the peridynamic formulation does not require any extraneous constitutive laws such as the kinetic relation (the relation between the velocity of the interface and the thermodynamic driving force acting across it) or the nucleation criterion (the criterion that determines whether a new phase arises from a single phase). Instead this information is obtained from inside the theory simply by specifying the inter-particle interaction. We derive a nucleation criterion by examining nucleation as a dynamic instability. We find the induced kinetic relation by analyzing the solutions of impact and release problems, and also directly by viewing phase boundaries as traveling waves.

We also study the interaction of a phase boundary with an elastic non-transforming inclusion in two dimensions. We find that phase boundaries remain essentially planar with little bowing. Further, we find a new mechanism whereby acoustic waves ahead of the phase boundary nucleate new phase boundaries at the edges of the inclusion while the original phase boundary slows down or stops. Transformation proceeds as the freshly nucleated phase boundaries propagate leaving behind some untransformed martensite around the inclusion.

© 2006 Elsevier Ltd. All rights reserved.

Keywords: Microstructures; Phase transformation; Shape-memory effect; Peridynamics; Stability and bifurcation

*Corresponding author. Tel.: +1 626 395 8306; fax: +1 626 568 2719.

E-mail addresses: kaushik@ugcs.caltech.edu (K. Dayal), bhatta@caltech.edu (K. Bhattacharya).

1. Introduction

The shape-memory effect consists of the recovery of apparently plastic deformations of a specimen below a critical temperature, by heating the specimen above this critical temperature. A diffusionless solid-state or martensitic phase transformation is responsible for this effect. The apparently plastic deformation does not come about by lattice slip, but instead is caused by the motion of twin or phase boundaries. It is the kinetics of this motion that is studied here.

In classical continuum theory, these phase transforming materials have been modeled using an energy that has multiple minima, each minimum corresponding to a particular phase or variant of martensite. In a dynamic, or even quasistatic, setting, the usual constitutive information, strain energy density as a function of strain, is insufficient to determine a unique solution. For example, even simple Riemann problems with a single phase or twin boundary in the initial conditions allow a one-parameter family of solutions. Therefore, we require further material information to pick the physically correct solution. [Abeyaratne and Knowles \(1990, 1991b\)](#) have proposed that this extra information may be specified in the form of a nucleation criterion and a kinetic relation.

The nucleation criterion determines whether a new phase will nucleate from a single phase. The kinetic relation determines the kinetics or the rules that govern the evolution of the phase boundary. It relates the velocity to a thermodynamic driving force, these being conjugate variables in the dissipation (or entropy) inequality. The driving force is related to Eshelby's idea of the force acting on a defect ([Eshelby, 1956, 1975](#)). The nucleation criterion and the kinetic relation provide uniqueness and well-posedness to initial-boundary value problems. Physically, they can be thought of as a macroscopic remnant of the lattice level atomic motion from one energy well to another that is lost in the continuum theory. However, a systematic derivation from a microscopic theory as well as experimental confirmation remain a topic of active research.

Another approach to overcome the inability of classical continuum mechanics to model the kinetics of phase transformations is to regularize or augment the theory, notably by adding a strain gradient (capillarity) and viscosity to the constitutive relation. This augmented theory leads to a unique solution for the motion of phase boundaries ([Abeyaratne and Knowles, 1991a; Truskinovsky, 1993](#)). Further, [Abeyaratne and Knowles \(1991a\)](#) have shown a correspondence between such methods and the kinetic relation. However, nucleation is incompletely explored in this theory, and computational evidence suggests that it is in fact quite difficult. Further, this theory leads to fourth-order equations which are difficult to deal with computationally: they are stiff and one needs smooth elements in the finite element method (see for example, [Kloucek and Luskin, 1994; Dondl and Zimmer, 2004](#)).

There is a closely related phase-field approach (see for example, [Artemev et al., 2001; Wang et al., 1994](#)) in the infinitesimal strain setting. Here, one uses the transformation strain as an internal variable or order parameter, considers the free energy density as a function of this order parameter and uses linear elasticity to penalize the incompatibility in this internal variable field. This leads to a second-order equation which is computationally attractive. However, the equilibrium and the dynamics can be different from that of the regularized theories described earlier ([Bhattacharya, 2003](#)). The connection between this theory and kinetic relations remains unexplored ([Killough, 1998](#) has some discussion on this question), nucleation remains difficult and most studies are quasistatic.

The peridynamic formulation is a nonlocal continuum theory that does not use the spatial derivatives of the displacement field (Silling, 2000; Silling et al., 2003; Kunin, 1982). Briefly, any two infinitesimal volume elements interact in this theory through a spring whose force depends on their position in the reference configuration and relative displacement. The same equations of motion are applicable over the entire body and no special treatment is required near or at defects. These properties make it a powerful tool to model problems that involve cracks (Silling and Kahan, 2004), interfaces, and other defects. This paper studies the kinetics of phase boundaries in the peridynamic formulation of continuum mechanics.

We introduce the peridynamic equation in one dimension in Section 2. We provide a constitutive relation that is the analog of the widely used trilinear material. We also propose a means of introducing viscosity into the peridynamic equations without introducing spatial gradients. We conduct quasistatic and dynamic numerical experiments in Sections 3 and 4, respectively. The absence of any spatial derivatives makes this relatively easy. Importantly, we find that phase boundaries nucleate and propagate naturally and uniquely in this theory with no need for any additional constitutive information like a kinetic relation or a nucleation criterion.

We examine nucleation in Section 5 by viewing it as a dynamic instability. This is different from the classical treatment of nucleation (Olson and Roitburd, 1992; Ball and James, 2005; Christian, 1975). In that treatment, one introduces perturbations with strains in the other well or phase (i.e., beyond the energy peak) and examines whether this perturbation lowers the total energy of the system. Our approach also differs from that of Abeyaratne and Knowles (1990), where the criterion for nucleation is based on the thermodynamic driving force.

In contrast, we examine conditions under which a single phase solution becomes dynamically unstable. Therefore, it is not necessary to have perturbations that reach into the other well (i.e., other stable phase). Instead, one can have nucleation when the strains reach the stability (convexity) limit of one phase. We are unaware of any other studies of nucleation from this viewpoint.

Our analysis introduces a notion of a defect size that has dimensions of length and is a measure of how many springs are in a stable state and how many are not. It depends on the physical region that is unstable, but also on how close the ambient strain is to the critical strain. We propose, based on stability considerations, that nucleation occurs when this defect size reaches a critical value, and show that this is consistent with our numerical simulations.

The kinetics of phase boundaries is examined in Section 6 by viewing the phase boundaries as traveling waves motivated by our numerical studies and following, Abeyaratne and Knowles (1991a), Purohit (2001) and Truskinovsky and Vainchtein (2005). We show that we can use these to derive a (viscosity-dependent) kinetic relation, and that this is consistent with the results of our numerical simulations.

We turn to two dimensions in Section 7. We propose a two-well constitutive relation that is appropriate for two variants generated by a square to rectangle transformation. We study the problem of a phase boundary driven towards a nontransforming elastic precipitate. Real materials often contain such defects. Indeed, in NiTi which is the most widely used shape-memory alloy, nickel- or titanium-rich precipitates are introduced to increase the plastic yield strength. We find that the phase boundary does not deviate from its planar configuration of preferred normal even when encountering the large residual

strain field of the precipitate. Further, in an intermediate range of driving force, we find that the phase transformation proceeds by nucleating a new phase boundary ahead of the inclusion while the original phase boundary stops behind it resulting in long slivers of untransformed material around the inclusions.

We conclude in Section 8 with a short discussion of our results.

2. Formulation in one dimension

The peridynamic equation of motion at a point in a homogeneous body is postulated to be (Silling, 2000)

$$\rho \partial_{tt} \mathbf{u}(\mathbf{x}, t) = \int_{\mathcal{R}} \mathbf{f}(\mathbf{u}(\mathbf{x}', t) - \mathbf{u}(\mathbf{x}, t), \mathbf{x}' - \mathbf{x}) dV_{\mathbf{x}'} + \mathbf{b}(\mathbf{x}, t), \quad (2.1)$$

where \mathbf{x} is the reference configuration coordinates, $\mathbf{u}(\mathbf{x})$ is the displacement field, $\mathbf{f}(\delta \mathbf{u}, \delta \mathbf{x})$ is the force between two volume elements with separation in the reference $\delta \mathbf{x} := \mathbf{x}' - \mathbf{x}$ and relative displacement $\delta \mathbf{u} := \mathbf{u}(\mathbf{x}', t) - \mathbf{u}(\mathbf{x}, t)$, $\mathbf{b}(\mathbf{x}, t)$ is the body force per unit volume in the reference and ρ is the density in the reference. We also refer to $\mathbf{f}(\delta \mathbf{u}, \delta \mathbf{x})$ as the spring force. This spring force is the constitutive input in the peridynamic formulation. See Silling (2000) for a discussion of the general properties of this formulation.

We specialize to a one-dimensional setting of a slab of infinite lateral extent and of length L undergoing uniaxial longitudinal deformations. The peridynamic equation of motion may now be written as

$$\rho \partial_{tt} u(x, t) = \int_0^L f(u(x', t) - u(x, t), x' - x) dx' + b(x, t). \quad (2.2)$$

We have to specify the spring force f . We assume that this spring force is of the form

$$f(\delta u, \delta x) = F \left(\frac{\delta u}{\delta x} \right) h(\delta x) \quad (2.3)$$

with h decaying rapidly. It is easily shown that this form ensures the right scaling for the energy in the large body limit. We may view $\delta u / \delta x$ as a pairwise strain measure, F as the strain-dependent force and h as the range-dependent strength of the interaction.

We model phase transforming materials by assuming that F has a trilinear form with two stable branches of equal modulus and one unstable branch with modulus equal in magnitude but negative. We assume that h decays with a length scale l_0 . Thus

$$f(\delta u, \delta x) = E \frac{\delta x}{l_0^3} e^{-(\delta x/l_0)^2} \times \begin{cases} \frac{4}{\sqrt{\pi}} \left(\frac{\delta u}{\delta x} + \varepsilon_0 \right) & \text{if } \frac{\delta u}{\delta x} \leq -\frac{\varepsilon_0}{2}, \\ \frac{4}{\sqrt{\pi}} \left(-\frac{\delta u}{\delta x} \right) & \text{if } -\frac{\varepsilon_0}{2} < \frac{\delta u}{\delta x} < \frac{\varepsilon_0}{2}, \\ \frac{4}{\sqrt{\pi}} \left(\frac{\delta u}{\delta x} - \varepsilon_0 \right) & \text{if } \frac{\delta u}{\delta x} \geq \frac{\varepsilon_0}{2}. \end{cases} \quad (2.4)$$

An advantage of this trilinear form is that it allows one to focus on phase boundaries which remain as the only nonlinearities. Note that $F(\delta u / \delta x)$ is dimensionless.

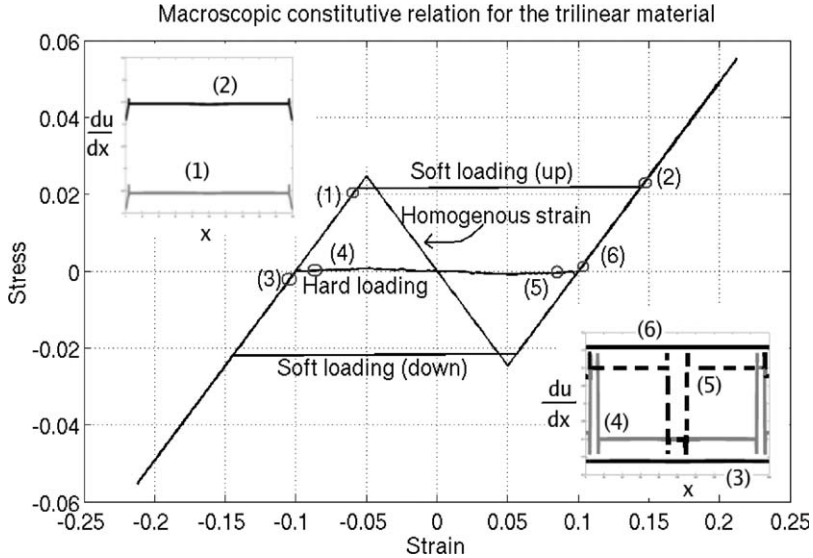


Fig. 1. The strain–stress curve for hard and soft loading, superposed over the homogeneous strain response.

To gain some insight into this relation, consider homogeneous deformations. It is possible to define a stress for such deformations (Silling, 2000). In one dimension, it is

$$\sigma(x) = \int_0^x \int_x^L f(u(x') - u(\hat{x}), x' - \hat{x}) dx' d\hat{x}. \tag{2.5}$$

We note for future use that in light of the decay, this formula may also be used whenever the deformation is homogeneous on a length-scale larger than l_0 . The macroscopic stress–strain curve for the microscopic force law in (2.4), calculated by assuming a homogeneous deformation, is shown in Fig. 1. We also define an elastic modulus for this material¹ using the expression $d\sigma/d\varepsilon$ and, not surprisingly, it is equal to the constant E in the stable low- and high-strain phases and $-E$ in the unstable phase.

While solving the initial-boundary value problem associated with the peridynamic equation of motion, we found that it would be useful to have a dissipative mechanism. The usual method of adding viscosity involves terms containing the strain rate (Abeyaratne and Knowles, 1991a), but this goes against the goal of peridynamics of eliminating spatial derivatives from the formulation. Hence, we add viscosity directly to the interaction force by transforming it in the manner $f \mapsto f + \nu(l_0/\delta x)\partial_t(\delta u/c)h(\delta x)$, where ν is the dimensionless coefficient of viscous damping, and $c = \sqrt{E/\rho}$ is the acoustic velocity in the long wavelength limit (see Weckner and Abeyaratne, 2005, for a discussion of dispersion in peridynamic materials). Lei et al. (2006) have used a similar formulation of damping in a different context.

¹This definition makes it equivalent to the classical elastic modulus in uniaxial deformation.

We now nondimensionalize the evolution equation and assign numerical values to the parameters that define the material. Multiplying (2.2) by l_0/E , we obtain

$$\begin{aligned} \frac{l_0}{c^2} \partial_{tt} u(x, t) &= \frac{l_0}{E} b(x, t) + \frac{l_0^2}{E} \int_0^{L/l_0} F\left(\frac{u(x', t) - u(x, t)}{x' - x}\right) h(x' - x) d\left(\frac{x'}{l_0}\right) \\ &+ \frac{\nu}{c} \frac{l_0^3}{E} \int_0^{L/l_0} \partial_t(u(x', t) - u(x, t)) \frac{h(x' - x)}{x' - x} d\left(\frac{x'}{l_0}\right). \end{aligned} \quad (2.6)$$

We set $\rho = 1$, $l_0 = 1$, $\varepsilon_0 = 0.1$ and $E = \sqrt{\pi}/4$ for the remainder of this paper. We usually set the length of the slab $L = 200$, but for faster phase boundaries we use longer slabs to allow the acoustic wave and phase boundary to be sufficiently distant for our analysis. Our results (nucleation and kinetics) are independent of L as long as $L \gg l_0$.

In the next couple of sections, we conduct numerical experiments with this material. We use a spatial discretization where we replace the integral over the body with a sum

$$\int_0^L f(u(x', t) - u(x_j, t), x' - x_j) dx' \approx \sum_{i=1}^N f(u_i(t) - u_j(t), x_i - x_j) \Delta x \quad (2.7)$$

and march forward in time with an explicit linear acceleration scheme. We use $\Delta x = 0.1$ for the spatial discretization, and the relation $\Delta x/\Delta t = 20\sqrt{E/\rho}$ for the time step so that we satisfy the CFL criterion for a classical wave equation with a large margin. We believe that since $l_0 \gg \Delta x$, this value of grid spacing is sufficient to approximate the integrals to be evaluated, and numerical tests show sufficient convergence of the results. A detailed numerical analysis would be interesting, but beyond the scope of this paper.

3. Quasistatics in one dimension

We begin our numerical exploration of the peridynamic trilinear material by studying the quasistatic response for both hard and soft loading. To obtain a quasistatic response, we start with an equilibrium state, increment the load or end displacement as appropriate, and solve (2.6) with a very large viscosity ν till such time that it reaches equilibrium, and iterate. Peridynamics requires some care for the application of the end conditions and their increment and these are discussed below. The results are shown in Fig. 1 superposed over the stress response for uniform strain fields.

3.1. Hard loading

We start these calculations with an equilibrium state with average strain deep in the low-strain phase. We apply successive increments of displacement using the boundary layers (rather than boundary points due to the nonlocal nature of peridynamics). Starting with the entire bar in the low-strain phase as described above, the relative displacement of the clamped ends is increased (equally but in opposite sense in the two ends to keep the calculation symmetric) to provide a given net strain increment to the bar. The strain in the clamped regions is also raised to correspond to this new average strain. The bar is then equilibrated by evolving the displacement field using the peridynamic equation of motion (2.6) with a large value of viscosity. The stress is calculated by using formula (2.5) at some point in the interior where the deformation is homogeneous. This procedure is repeated by raising the strain until the entire bar is completely in the high-strain phase. The strain is

subsequently reduced in a similar manner till the bar returned to its original low-strain state. The results are shown in Fig. 1 along with the strain (du/dx) profiles at selected points.

We see that the material leaves the low-strain curve close to the so-called Maxwell stress, suffers strain increments at constant stress till it reaches the high-strain curve and then follows it. It behaves analogously as the strain is lowered. Recall that the Maxwell stress is defined as the stress at which the net signed area between the horizontal line and a stress–strain curve is zero and corresponds to the value of stress at which the exchange of absolute stability occurs between the low- and high-strain phase. The strain field corresponding to point (3), before nucleation, shows uniform strain in the bar. The strain field corresponding to point (4), soon after nucleation, shows that phase boundaries nucleate at the ends of the bar. There are two pairs of phase boundaries, one at each end. The strain away from the phase boundary is close to the equilibrium values of the two phases. The outer phase boundary at each end remains fixed in position at the grips while the inner one migrates as the applied displacement increases. The strain field corresponding to point (5), shows the inner phase boundaries about to meet each other. The strain field point (6) shows that the bar is entirely in the high-strain phase. A similar process takes place on the downward path.

Note from the insets that the strain fields show an overshoot and an undershoot around the phase boundary as it transitions between the two states. This is a common feature of models of phase transitions, for example, in Purohit (2001) and Zimmermann (2002). We shall study the detailed structure of the phase boundaries in subsequent sections.

3.2. *Soft loading*

Soft loading calculations are performed by applying a uniform body force in the boundary layers as described in Silling (2000). We start with a body force that causes sufficient compression for the entire bar to be in the low-strain phase. The body force is increased incrementally, the bar is equilibrated after each increment by solving (2.6) with large dissipation, and the procedure repeated till the entire bar is in the high-strain phase. Subsequently, the stress is incrementally decreased in a similar manner till the bar returns to its initial low-strain state. The resulting stress–strain curve as well as the strain field in the bar at points marked (1) and (2) on the stress–strain curve are shown in Fig. 1.

The average strain is seen to follow the low-strain phase until almost the peak stress. Phase boundaries nucleate at the ends of the bar, at the strain singularities, and move at high velocity to meet at the center and transform the entire bar into the high-strain state. This nucleation and meeting of the phase boundaries occurs within one load step (1% of the peak-to-valley stress difference). The material then follows the stress response curve of the high-strain phase. A similar sequence occurs on the downward path.

We discuss the differences in the hard and soft loading response in Section 5 after we have looked at dynamic situations.

4. **Dynamic phase boundaries in one dimension**

We now study the initial-boundary value problem associated with (2.2) and solve by marching forward in time. We consider two classes of problems, release (Riemann) and impact. These classes of problems play an important role in the classical theory: having

solutions to them assures existence of solutions to all initial-boundary value problems (Lefloch, 1993).

4.1. Release problems

In the release or Riemann problem, we seek to study the evolution of the displacement from a piecewise affine initial condition. To set up the initial condition, we obtain an equilibrium strain field with a phase boundary and then transform it using $\varepsilon(x) \mapsto A\varepsilon(x) + B$ so that we obtain a piecewise constant but unequilibrated strain field with a nonzero driving force across the phase boundary. The boundary conditions are applied through clamped regions with the strain held uniform and constant at the initial value.

The calculations are performed for various initial driving forces across the interface. Sequences of snapshots of the displacement fields for low-, moderate- and high-driving forces are shown in Fig. 2 for both viscous ($\nu = 0.333$) and inviscid materials. The overall structure of the solution is shown in Fig. 3(a). The movement of the phase boundary can be easily followed from the displacement field by noting that the high-strain phase has positive strain and thus positive slope, and the low-strain phase has negative strain and thus negative slope. A change in slope without change in sign of the slope indicates an acoustic wave. All the calculations shown involve the original phase boundary moving to the left and the displacement increasing with time.

Since the initial phase boundary is not at equilibrium, it begins moving in the direction of the driving force, sending out acoustic waves in both directions. The phase boundary evolves to a steady profile quite rapidly. The acoustic waves that are sent out by the phase boundary hit the clamped ends of the bar, and reflect back into the domain. They may also nucleate phase boundaries at the ends of the bar. These phase boundaries then move back into the interior of the bar. Depending on the average strain in the bar (imposed through the initial conditions by the clamping positions of the ends of the bar), the phase boundaries can merge and form an entirely low- or high-strain bar, or equilibrate to some mixture of high- and low-strain phases.

One feature of the solution that can be seen in Fig. 2 is that viscosity plays an important role in removing the short wavelength oscillations behind the phase boundary. As is expected in the peridynamic theory, these short waves have very small velocity (Silling, 2000). Using dissipation to remove them helps clarify the displacement field without changing the kinetics significantly. Viscosity also seems to encourage nucleation at the clamped boundaries of the bar, as can be seen by comparing Figs. 2(a) and (b).

We also observe from our solutions that the phase boundaries travel at constant velocity (after an initial startup stage) and maintain their shape. We examine whether the motion of these interfaces follow a kinetic relation as postulated by Abeyaratne and Knowles (1991b). To this end, we calculate the driving force across the phase boundary defined as (Abeyaratne and Knowles, 1991b)

$$F = \llbracket W(\varepsilon) \rrbracket - \frac{1}{2}(\sigma(\varepsilon_+) + \sigma(\varepsilon_-)) \llbracket \varepsilon \rrbracket, \quad (4.1)$$

where $\llbracket g \rrbracket := g_+ - g_-$ is the jump across the phase boundary of the quantity g , W is the stored elastic energy, σ is the stress, and ε is the strain. Since the phase boundary in the peridynamic formulation is not a sharp interface separating two regions of uniform deformation as in the conventional continuum theory, we use the average of the strain fields on either side of the phase boundary (ensuring that there are no other waves within

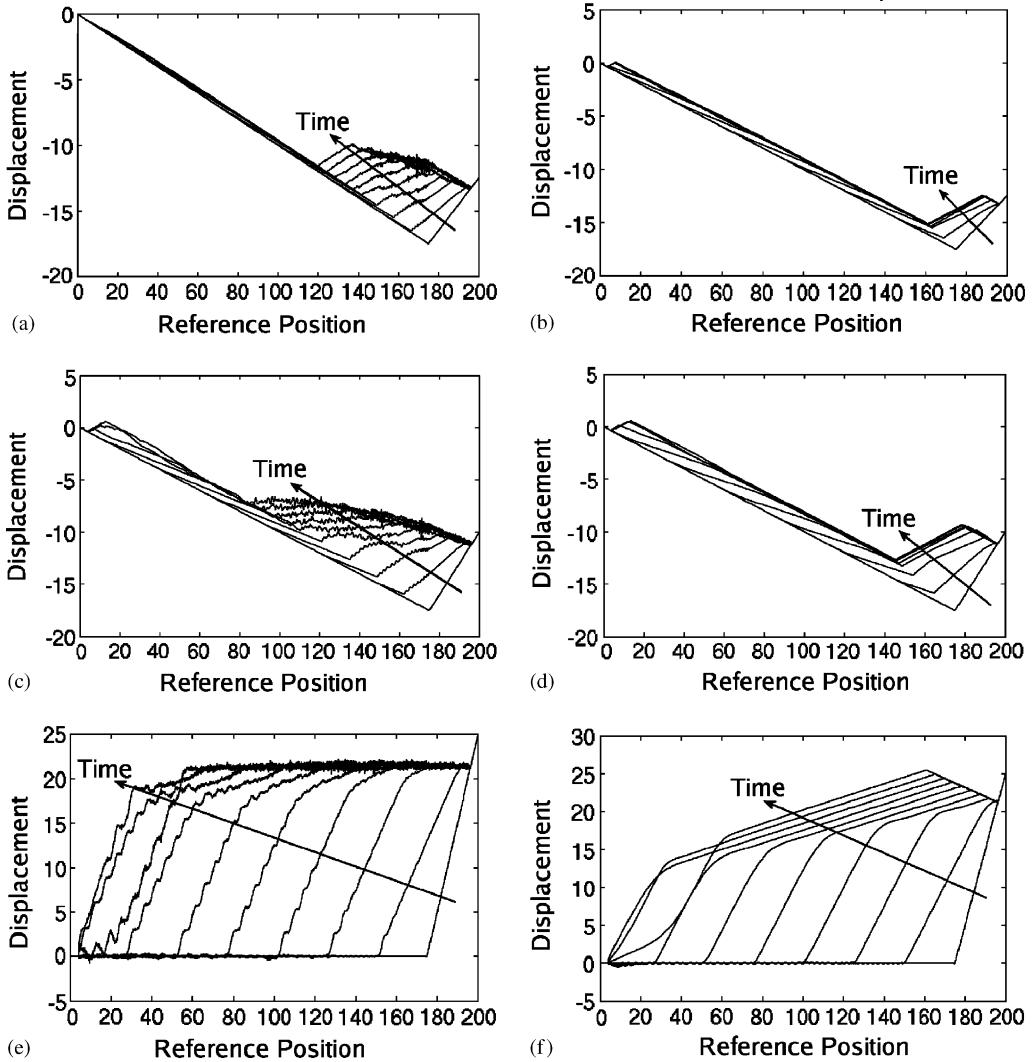


Fig. 2. Snapshots of the displacement field in the release problem. (a) Low-driving force, inviscid, (b) low-driving force, viscous, (c) moderate-driving force, inviscid, (d) moderate-driving force, viscous and (e) high-driving force, inviscid, (f) high- driving force, viscous.

the averaging window). We plot driving force F (normalized by E) versus velocity v (normalized by c , $M = v/c$) in Fig. 4. The results of various release calculations appear to collapse onto a single curve. This suggests that the peridynamic theory does in fact induce a kinetic relation. We shall return to study this curve in Section 6.

4.2. Impact problem with initial phase boundary

We now turn to impact problems where an equilibrium strain field with a phase boundary in the interior is used as initial condition. One end of the bar is clamped, and the

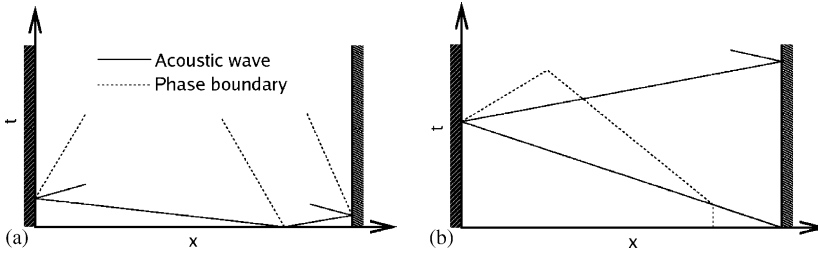


Fig. 3. Schematic $x-t$ plane diagram for the release and impact problems: (a) release problem and (b) impact problem.

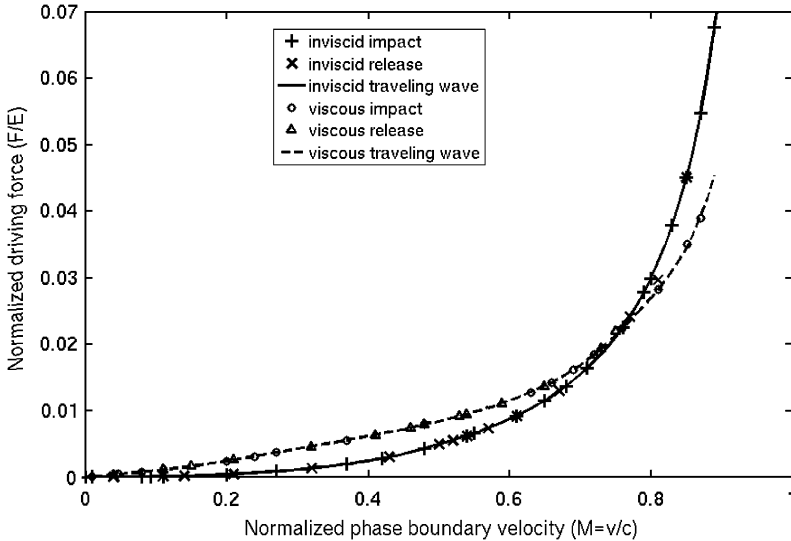


Fig. 4. The kinetic relation induced by peridynamics. The points are results extracted from the dynamic simulations whereas the curves are the results of traveling wave calculations.

other end is pulled at a constant velocity for all $t > 0$. The clamped end has uniform and constant strain equal to the equilibrium strain at $t = 0$ and this region is not evolved in time. The pulled end is subjected to a constant and uniform velocity, so that its strain remains constant and uniformly equal to the other equilibrium strain at $t = 0$.

Snapshots of the displacement fields for low-, moderate- and high-impact velocities are shown in Fig. 5 for both viscous ($\nu = 0.333$) and inviscid materials. The overall features of the solution are shown in Fig. 3(b). The phase boundaries and acoustic waves can be identified and followed as described in the release problem. The ordering of the displacement fields in time can be seen by looking at the right end of the bar, that is being pulled at a constant positive velocity. The greater the displacement at the right end, the further in time the snapshot.

The initial impact sends an acoustic wave into the bar, which reaches the phase boundary and sets it into motion. The acoustic wave then goes ahead of the phase

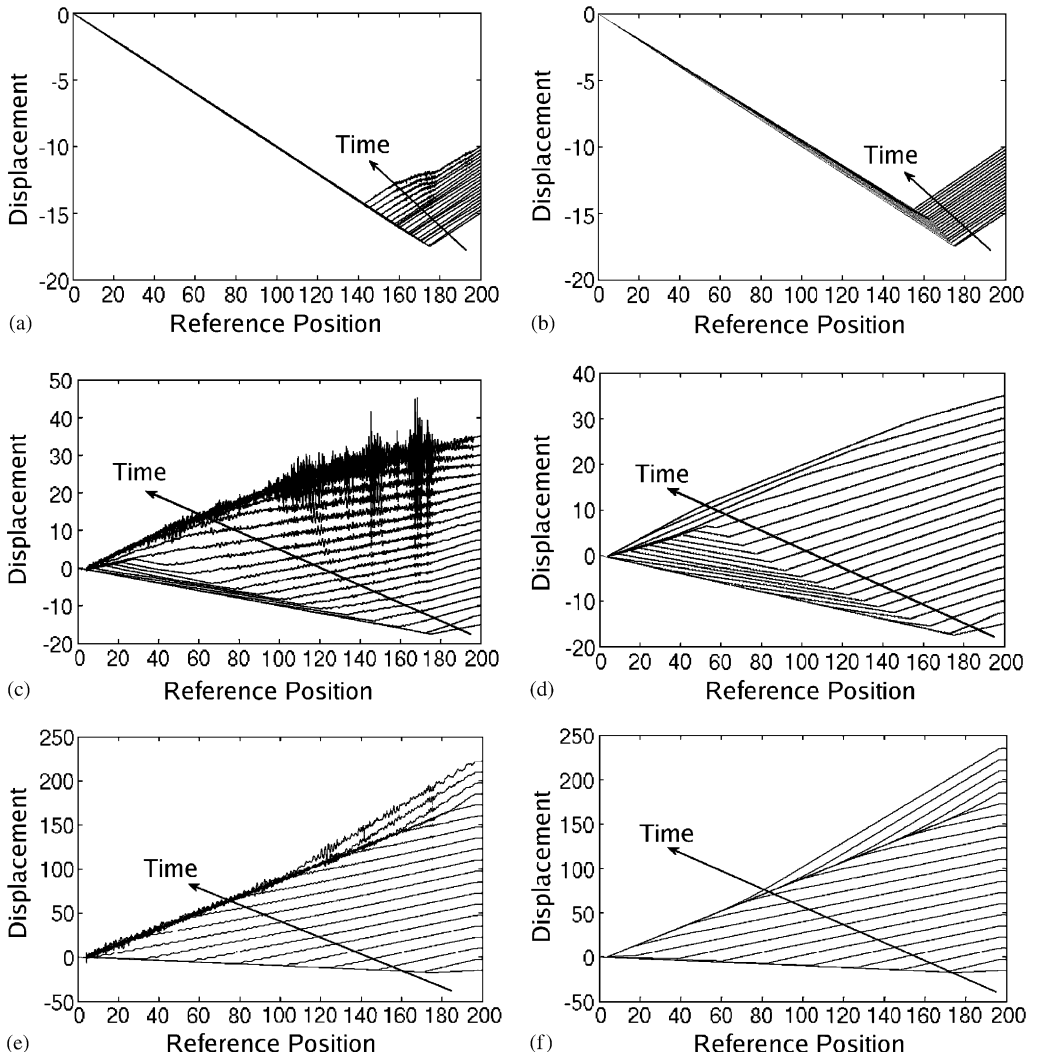


Fig. 5. Snapshots of the displacement field in the impact problem with initial phase boundary. (a) Low velocity, inviscid, (b) low velocity, viscous, (c) moderate velocity, inviscid, (d) moderate velocity, viscous, (e) high velocity, inviscid and (f) high velocity, viscous.

boundary and reaches the clamped end, where it reflects back into the bar, possibly nucleating another phase boundary there. The second phase boundary, when it exists, moves behind the acoustic wave and meets the original phase boundary and they annihilate each other leaving the entire bar in a high-strain state. If the second phase boundary does not nucleate, the original phase boundary reaches the end of the bar, again leaving the entire bar in the high-strain state.

As in the release problem, viscosity plays a role in removing the short wavelength oscillations without changing the kinetics greatly.

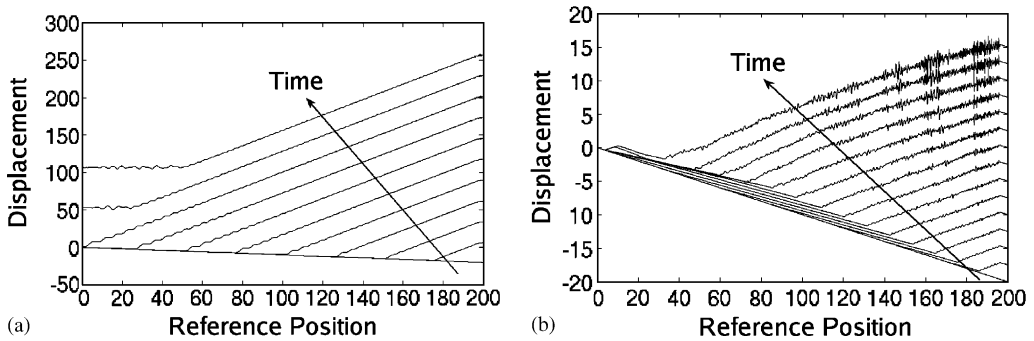


Fig. 6. Snapshots of the displacement field in the inviscid impact problem without initial phase boundary. (a) Stress control and (b) displacement control.

Finally, the phase boundaries propagate steadily with fixed structure after an initial transient, and by plotting the driving force versus velocity in Fig. 4, we see that they follow the same kinetic relation as the release problems.

4.3. Impact problem without initial phase boundary

We finally turn to impact problems with initial conditions involving a uniform strain field. We set the strain equal to the low-strain equilibrium value in the entire bar. We find that weak impact results in just an acoustic wave traveling into the bar, but a sufficiently strong impact causes the nucleation of a phase boundary at the impacted end. The displacement fields for impact experiments with different boundary conditions is shown in Fig. 6.

Fig. 6(a) shows an inviscid bar completely in the low-strain phase, subjected to a tensile stress (soft loading) at the right end and left free at the left end. The tensile stress is applied as a step loading, and this causes an acoustic wave and a phase boundary to nucleate at the shocked end. The acoustic wave travels faster than the phase boundary till it reaches the far free end, and bounces off without nucleating any new phase boundary.

Fig. 6(b) shows an inviscid bar completely in the low-strain phase, subjected to a displacement controlled extension with the far end clamped. We see, as before, that an acoustic wave and a phase boundary are nucleated at the impact side of the bar. The acoustic wave nucleates an additional phase boundary when it bounces off the far end that is clamped, in contrast to the previous case where no nucleation occurred at the free end.

We explain the reason for the different nucleation behavior under different clamping conditions in Section 5 after we formulate a nucleation criterion.

5. Nucleation as a dynamic instability

The numerical experiments in the previous sections show that nucleation occurs naturally from within the peridynamic theory. Further, the nucleation behavior is varied but very important in determining the overall behavior: recall the contrast between the hard and soft loading or the difference between the clamped and free end. We therefore

seek to understand the conditions under which nucleation occurs by examining the point of view that nucleation occurs as a result of a dynamic instability.

We study the nucleation of the high-strain phase from the low-strain phase and note that the reverse transformation is completely analogous. Further, we modify the constitutive relation (2.4) slightly by translating the strain axis so that the boundary between the low-strain and unstable branches occurs at $\varepsilon_0/2$ (instead of at $-\varepsilon_0/2$). We note that this modification is simply a change of variables for convenience and does not affect any results. Finally, we only consider the low-strain and unstable branches because we are only interested in the rate of growth of a perturbation from the low-strain phase for small times.

While our numerical calculations involved finite slabs, the lengths of the slabs were much larger than the intrinsic peridynamic interaction length. For the analysis in this section, we treat the slabs as being of infinite length.

Consider a displacement field $u(x, t)$ evolving according to the peridynamic equation of motion. It is easy to verify that this solution remains linearly stable as long as all springs remain in the low-strain region. So let us consider a time when most springs are in the low-strain region but some springs have reached beyond the limit and into the unstable region. We call such a displacement field a *defect*, and examine its linear stability. We call it a *stable defect* if it is linearly stable and an *unstable defect* if it is linearly unstable. Note that all defects—stable and unstable—contain some springs that are in the unstable region. But stable defects are stable despite that. We postulate that unstable defects lead to nucleation.

We perturb the displacement field $u(x, t) \mapsto u(x, t) + \varepsilon v(x, t)$ and study the evolution of this perturbed field. Substituting this in the governing equation (2.2) and differentiating with respect to ε gives us the linearized equation in $v(x, t)$

$$\partial_{tt}v(x, t) = \int_{\mathbb{R}} f_{,1}(u(x', t) - u(x, t), x' - x) (v(x', t) - v(x, t)) dx', \tag{5.1}$$

where $f_{,1}(u(x', t) - u(x, t), x' - x)$ is the derivative of $f(\cdot, \cdot)$ with respect to the first argument and evaluated at $(u(x', t) - u(x, t), x' - x)$. For conciseness, we denote $f_{,1}(u(x', t) - u(x, t), x' - x)$ by $C_u(x, x')$, and we note that $C_u(x, x') = \pm e^{-(x'-x)^2}$ with the plus sign for stable springs and the minus sign for unstable springs.

By separation of variables we find that $v(x, t) = v(x)e^{i\omega t}$, where ω and $v(x)$ are given by the following eigenvalue problem:

$$\omega^2 v(x) = \int_{\mathbb{R}} C_u(x, x')(v(x) - v(x')) dx' =: L_u[v(x)]. \tag{5.2}$$

If ω is real or if it contains only positive imaginary part, then the solution u is stable. The solution is unstable if it has a negative imaginary part.

It is easy to verify using standard methods in integral equations (see for example, Porter and Stirling, 1990) that the operator L_u is self-adjoint in the Hilbert space of locally square integrable functions. It follows that all its eigenvalues ω^2 are real. Therefore the stability of the solution u reduces to examining the smallest eigenvalue of L_u : the solution u is unstable if the smallest eigenvalue is negative and stable otherwise. Further, the smallest eigenvalue can be posed as a variational problem of finding the minimum of

$$I(v) = \int_{\mathbb{R}^2} C_u(x, x')(v(x)^2 - v(x')v(x)) dx' dx \tag{5.3}$$

over all functions v with

$$\int_{\mathbb{R}} v^2 dx = 1. \tag{5.4}$$

To evaluate the functional I above, it is important to identify which springs are in the stable phase and which are not. This is not straightforward to identify for an arbitrary displacement field $u(x)$ since this depends on the displacement of two distant points that are connected by the spring. So it is natural to work in the two-dimensional space x versus x' shown in Fig. 7(b). We divide this space into stable and unstable regions: a point (x, x') is in the stable region if the spring connecting x and x' is stable, and in the unstable region otherwise. Assuming that the unstable regions are localized, we have the picture shown in Fig. 7(b) based on two lengthscales: a lower lengthscale δ^l such that all springs with both $|x| < \delta^l, |x'| < \delta^l$ are unstable and $C_u(x, x') = -e^{-(x'-x)^2}$, and an upper lengthscales δ^u such that all springs with either of $|x|, |x'| > \delta^u$ are stable and $C_u(x, x') = e^{-(x'-x)^2}$. The values of δ^l, δ^u and hence the sizes of the different regions in the spring-space will depend on the shape of the defect.

We begin our consideration with a special displacement field $u(x)$ that we call the *ideal defect*, where $\delta^l = \delta^u = \delta$. This displacement field is shown in Fig. 7(a), with slope $u'(x) \leq \epsilon_0/2$ for $|x| > \delta$, and a uniform slope $u'(x) = \epsilon_0/2$ for $|x| < \delta$. In other words, we are in the stable low-strain phase except for an interval of length 2δ , where we are at the limiting strain that separates the low-strain from the unstable phase. We examine the stability of the ideal defect and then use it to obtain bounds on the behavior of a general displacement field.

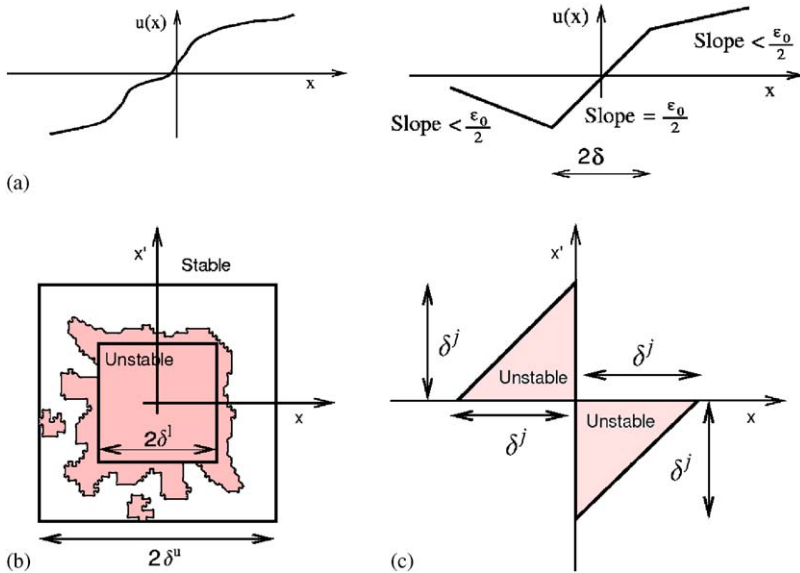


Fig. 7. Defect geometries and spring space maps. (a) The displacement fields of a typical and ideal defect. (b) The two-dimensional spring-space associated with typical defects. The springs connecting (x, x') in the shaded region are unstable and the others are stable. (c) The two-dimensional space associated with a jump defect.

The linear operator associated with the ideal defect is

$$L_\delta[v(x)] := \int_{\mathbb{R}} e^{-(x'-x)^2} (v(x) - v(x')) dx' + 2H(\delta - |x|) \left(-v(x) \int_{(-\delta, \delta)} e^{-(x'-x)^2} dx' + \int_{(-\delta, \delta)} e^{-(x'-x)^2} v(x') dx' \right),$$

where $H(y)$ is the unit Heaviside step function that is 0 for $y < 0$ and 1 for $y > 0$ and functional (5.3) becomes

$$I_\delta(v) = \int_{\mathbb{R}^2} e^{-(x'-x)^2} (v(x)^2 - v(x)v(x')) dx dx' - 2 \int_{(-\delta, \delta)^2} e^{-(x'-x)^2} (v(x)^2 - v(x)v(x')) dx dx'. \tag{5.5}$$

By setting $\delta = 0$, we see that $I_0 > 0$. Further one can use Fourier analysis to show that the minimum of I_δ is continuous with respect to δ at $\delta = 0$. So we expect the ideal defect to be stable for small δ . Further, setting $\delta \rightarrow \infty$, we see that $I_\infty < 0$. Therefore, we anticipate that the ideal defect becomes unstable beyond some finite δ .

To understand this further, we examine (5.5) above for a finite δ . We expect the minimum to be achieved for functions v that are strongly localized near the origin so that the second term dominates. Physically, we are exciting primarily the unstable springs near the origin while exciting as few stable springs as possible. For such a function,

$$\begin{aligned} I_\delta(v) &= \pi^{1/2} + \int_{(-\delta, \delta)^2} e^{-(x'-x)^2} v(x)v(x') dx dx' \\ &\quad - \pi^{1/2} \int_{(-\delta, \delta)} (\text{erf}(x + \delta) - \text{erf}(x - \delta))v(x)^2 dx \\ &\approx \pi^{1/2} + \int_{(-\delta, \delta)^2} v(x)v(x') dx dx' - 2\pi^{1/2}\text{erf}(\delta) \int_{(-\delta, \delta)} v(x)^2 dx \end{aligned}$$

by approximating the values of the integrands near $x = 0, x' = 0$. Using the fact that the double integral above is now decoupled into two single integrals that are equal, we can write the double integral as a square and hence it is positive. Since v is localized, we can extend the range of integration in the second integral to all space, and then use (5.4) to conclude that this second integral is equal to one. Therefore,

$$\begin{aligned} I_\delta(v) &\geq \pi^{1/2}(1 - 2\text{erf}(\delta)) \\ &\geq 0 \quad \text{if } \text{erf}(\delta) \leq \frac{1}{2} \Leftrightarrow \delta \lesssim 0.477. \end{aligned} \tag{5.6}$$

This provides an upper bound for the size of a stable ideal defect. Numerical computations below show that this bound is in fact attained. Thus we conclude that the ideal defect is stable if $\delta \leq \text{erf}^{-1} \frac{1}{2} \approx 0.477$ and unstable for larger δ .

For the numerical computations, we consider an infinite bar and discretize the operator L_δ as

$$\begin{aligned} (L_\delta)_{ij} &= \delta_{ij}\pi^{1/2}(1 + H(\delta - |x_i|)(\text{erf}(x_i - \delta) - \text{erf}(x_i + \delta))) \\ &\quad - e^{-(x_i-x_j)^2} \Delta x + 2H(\delta - |x_i|)H(\delta - |x_j|)e^{-(x_i-x_j)^2} \Delta x \end{aligned} \tag{5.7}$$

and use standard numerical algorithms (Anderson et al., 1999) to find the smallest eigenvalue. Notice that zero is always an eigenvalue for the original (continuous) operator

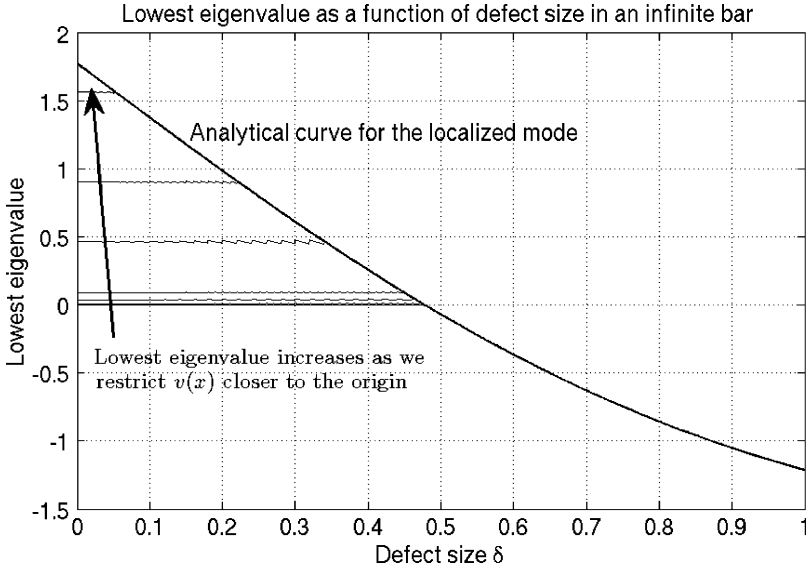


Fig. 8. Numerical calculation of the lowest eigenvalue.

with rigid translation as the eigenmode. While rigid translation is not square-integrable on infinite domains, it alerts us to the fact that the infimum of the spectrum may in fact be zero. Therefore we look for eigenmodes with finite support and the results are plotted in Fig. 8, where the support of v is limited to the intervals $(-100, 100)$, $(-10, 10)$, $(-5, 5)$, $(-3, 3)$, $(-1, 1)$, $(-0.5, 0.5)$ and $(-0.1, 0.1)$. For small defect size δ the smallest eigenvalue is positive (with the value depending on the support of v) and remains constant² with δ . We have found that the eigenmode associated with this eigenvalue is an approximation to the rigid translation mode of the original (continuous) operator. This remains the smallest eigenvalue with increasing defect size δ till a critical value where it crosses the eigenvalue associated with what eventually becomes the localized unstable mode. The eigenvalue associated with this mode is monotone decreasing with δ , insensitive to the constraint on the support of v , follows closely the analytic predictions above and becomes negative at $\delta \approx 0.477$. We have obtained similar results with a second discretization based on a bar of finite length; the lowest eigenvalue is zero with rigid body eigenmode until the localized mode becomes unstable.

We now turn to the general defect. We show in Appendix A that the results above for the ideal defect can be used to obtain bounds on the stability of any general defect with radii δ^l, δ^u . It follows that any defect is stable if $\text{erf}(\delta^u) < \frac{1}{2}$ and any defect is unstable if $\text{erf}(\delta^l) > \frac{1}{2}$.

Finally, we turn to a defect that consists of a displacement jump. The solutions of the peridynamic equations may contain a displacement discontinuity, for example, when the initial displacement, initial velocity or applied body force contain such a discontinuity (Weckner and Abeyaratne, 2005). In fact, we encountered such discontinuities in our numerical experiments earlier.

²The small oscillations are discretization artifacts and we have verified that they go away with refinement.

Consider a displacement field with uniform strain $\bar{\epsilon} (< \epsilon_0/2)$ with a jump discontinuity at the origin. It is easy to find the stable and unstable springs and this is shown in Fig. 7(c) with

$$\delta^u = \delta^j = \frac{[[u]]}{\Delta\epsilon}, \quad \delta^l = 0, \quad (5.8)$$

where $\Delta\epsilon = \epsilon_0/2 - \bar{\epsilon}$. Since $\delta^l = 0$, we cannot directly apply the bounds in Appendix A. We instead study it numerically to find the critical value of δ^j (≈ 0.75) below which the jump defect is stable and beyond which it is unstable.

Eq. (5.8) reveals an important scaling property of peridynamics. It shows that the defect size depends on how far the ambient strain field is from the critical strain ($\Delta\epsilon$). We show in Appendix B that this is not the case in the traditional regularized theories.

With the stability results in hand, we consider a series of dynamic calculations using the original constitutive relation (2.4) to probe the applicability of these stability considerations to nucleation in fully nonlinear calculations. The first set of calculations consists of initial condition with a bar with uniform strain in the low-strain phase and with a single displacement continuity. We consider various initial strains and jumps and catalog when they lead to nucleation and when they do not. We find that there is no nucleation when the initial defect size $[[u]]/\Delta\epsilon$ is smaller than 1.0, but nucleation whenever it exceeds it. This confirms the scaling predicted by linear stability considerations, though the critical value is larger than predicted. The second set of calculations consists of initial conditions with uniform strain but discontinuous velocity. Once again we vary the initial strain and velocity jump and catalog when they lead to nucleation and when they do not. These calculations again confirm the scaling predicted by the stability criterion, though the critical defect size is 0.42.

The third and final set of calculations consist of initial conditions with uniform strain but subjected to discontinuous body force. Repeating the calculations for various initial strains and body force jumps, we again find that the scaling agrees very well. We note that in this case, nucleation does not depend only on the size of the discontinuity in the body force, but also the extent of the region over which the body force is applied (as this is related to the total force applied on the body and strongly influences the evolution of the surrounding strain field). For a few different sizes of region of application (with the body force being constant within these regions), we obtain the same scaling with initial strain field, but of course the size of the critical defect varies depending on the size of the application region.

In summary, we find that the stability calculations correctly identify the defect size to be the entity which determines nucleation. However, the value of the critical defect size may depend on the particular situation. One reason for this is that a displacement discontinuity in a peridynamic theory is fixed in space but evolves with time according to a simple second-order equation (Weckner and Abeyaratne, 2005):

$$\frac{d^2}{dt^2} [[u]] + \sqrt{\pi} [[u]] = [[b]]. \quad (5.9)$$

Thus if we start with a displacement discontinuity but no velocity discontinuity in the initial condition, the magnitude of the displacement discontinuity decreases with time before the instability has time to develop. Hence, we expect the stability criterion applied to the initial condition to over-predict nucleation as we find above. In contrast when one

has an initial velocity but no displacement discontinuity, the displacement discontinuity as well as the ambient strain grow with time and thus we anticipate our stability condition to under-predict the instability as we find above.

We conclude this section by revisiting the numerical experiments in the previous sections. In the quasistatic hard loading, each displacement increment gives rise to a displacement jump of $\llbracket u \rrbracket = 0.200$. We then expect nucleation to occur when the difference between the unstable strain and the ambient strain $\Delta\varepsilon$ reaches $0.2/\delta^{\text{crit}}$. On the increasing half-cycle, this corresponds to a value of ambient strain smaller than $\varepsilon = -0.25$ which is smaller than the smallest strain considered. So we conclude that nucleation occurs at each displacement increment in that calculation. However, as long as we are below the Maxwell stress, we expect the newly nucleated phase boundaries to be driven out of the bar during the subsequent equilibration. Thus we expect phase transformation to begin at the Maxwell stress and this is exactly what we see in Fig. 1. We have verified our argument by examining the transients in our calculations. Further, these calculations show that we can control the point at which phase transformation begins by taking smaller displacement increments so as to create smaller displacement jumps; we have verified this numerically.

In the case of quasistatic soft loading, we note that nucleation occurs close to the peak but not exactly at the peak. If we compare the defect radius at the load step just before nucleation, and the point on the curve that the bar would reach had nucleation not taken place, we see that we obtain a critical nucleation outer radius between 0.505 and 0.530 in agreement with our earlier result.

In the impact problem without an existing phase boundary, recall that a new phase boundary was nucleated at the far end by the acoustic wave when that end is clamped but not when that end is free. With a clamped end, the impinging acoustic wave creates a velocity discontinuity that in turn leads to a displacement discontinuity and thus nucleation. In contrast, with a free end, there is no defect created and there is no nucleation.

In summary, we find that linear instability of the dynamic solution is an accurate predictor of nucleation.

6. Phase boundaries as traveling waves

A noticeable feature of the numerical solutions to dynamic problems that we obtain in Section 4 is that the phase boundaries appear to have an invariant shape and move at a constant velocity. Hence, we seek a solution to (2.2) in the form of a traveling wave

$$u(x, t) = u(x - vt) \quad (6.1)$$

that connects the two phases. Substituting (6.1) in (2.2), the governing equation becomes³

$$M^2 \left(\frac{d^2 u(y)}{dy^2} \right) = \left(\frac{1}{E} \int_0^L f(u(y'), y' - y) dy' \right), \quad (6.2)$$

where $M = v/c$ and $y := x - vt$ is the coordinate in the translating frame that moves with the phase boundary at a constant velocity v . The second derivative on the left hand side would seem to impair the ability of peridynamics to be valid at all points in the body,

³We have assumed that our computational window is translating with the phase boundary, and the limits of the integral are correspondingly changed.

including at singularities. However, we note the result of [Weckner and Abeyaratne \(2005\)](#) that a displacement or velocity discontinuity has a fixed position at all time. As we are working in a translating frame that moves with a constant velocity v , such discontinuities are not allowed to exist in $u(y)$, and we can define a weak second derivative.

The discretization in space is given by

$$\int_0^L f(u(x', t) - u(x_j, t), x' - x_j) dx' \approx \sum_{i=1}^N f(u_i(t) - u_j(t), x_i - x_j) \Delta x, \tag{6.3a}$$

$$\frac{d^2 u(y)}{dy^2} \approx \frac{u_{j+1} - 2u_j + u_{j-1}}{(\Delta y)^2} \tag{6.3b}$$

and we have used $\Delta x = 0.1$ as before.

We now attempt to solve the traveling wave problem by assuming a value for M and finding the associated displacement field. From the displacement field, we can find the strain field and hence the driving force associated with this M .

To find the displacement field, we divide the domain $\mathcal{B} := \{y : y \in [0, L]\}$ into an interior $\mathcal{I} := \{y : y \in [L_{bc}, L - L_{bc}]\}$, a left boundary layer $\mathcal{B}_- := \{y : y \in [0, L_{bc}]\}$, and a right boundary layer $\mathcal{B}_+ := \{y : y \in [L - L_{bc}, L]\}$. We define the residue $R(u(y)) := [M^2(d^2 u(y)/dy^2) - ((1/E) \int_0^L f(u(y') - u(y), y' - y) dy')]$. We aim to minimize the 2-norm of the residue over the interior \mathcal{I} :

$$\min \int_{\mathcal{I}} R(u(y))^2 dy \approx \min \sum_{u(y_i) \in \mathcal{I}} R(u(y_i))^2. \tag{6.4}$$

Our initial approach was to minimize the norm of the residual (normalized with respect to the height of the energy barrier and length of the computational domain) on \mathcal{I} over the set of displacements $u(y_i)$, where $y_i \in \mathcal{I}$ and assuming constant strain fields in $\mathcal{B}_-, \mathcal{B}_+$ by extrapolating. As M increases, the constant strain approximation does not work. Instead, we minimize the norm of the residual on \mathcal{I} over the entire set of displacements $u(y_i)$, where $y_i \in \mathcal{B}_- \cup \mathcal{I} \cup \mathcal{B}_+$. This allows us to capture the oscillations around the phase boundary. A singularity is formed at the interface of the boundary layer with the interior, and is analogous to the singularity expected when the applied body force changes sharply in space ([Silling et al., 2003](#)), if we think of the error minimization process in terms of a fictitious body force applied in the boundary layers.

The minimization is performed using a standard conjugate gradient algorithm ([Anderson et al., 1999](#)). We start with a static phase boundary (i.e., $M = 0$), and use this as the initial guess for a phase boundary moving at a low M . Once we have found this phase boundary, it is then used as an initial guess for a slightly faster phase boundary. This procedure is repeated till we come as close to $M = 1$ as possible. For phase boundaries that are very close to $M = 1$, the conjugate gradient solver is unable to find a solution that connects the two phases and instead finds solutions that are single phase.

With viscosity ($\nu = 0.333$), the traveling wave calculations yield the kinetic relation shown as dashed line in [Fig. 4](#). It coincides with that obtained from dynamic calculations with the same value of viscosity in the previous section. A typical traveling wave profile (at $M = 0.33$) is shown in [Fig. 9\(a\)](#).

For the inviscid material, however, the situation is different. We still obtain traveling waves but the displacement field is quite different from those observed in dynamic

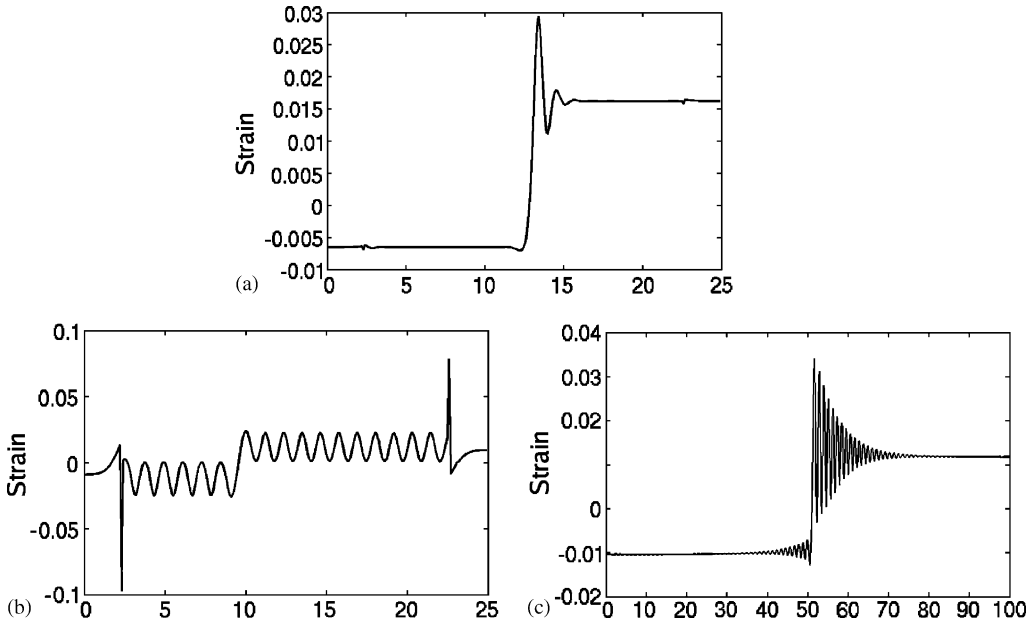


Fig. 9. Strain fields from the traveling wave calculations at $M = 0.33$. Note the different scales: (a) viscous ($\nu = 0.333$), (b) inviscid and (c) almost inviscid ($\nu = 0.005$).

calculations. One has sinusoidal waves of a specific frequency that do not die out but persist over all space with constant amplitude as shown in Fig. 9(b). Similar solutions have been found by Zimmermann (2002). Further, they are symmetric, i.e., the strain fields on either side of the phase boundary are reflections of each other around the zero-strain line. Consequently, it follows from (4.1) that the driving force is zero. Thus the kinetic relation is a horizontal line $F = 0$, again differing from the dynamic calculations.

To explore this issue further, we break the symmetry of the displacement field for an inviscid phase boundary by adding viscosity, and study the limiting kinetic relation as $\nu \rightarrow 0$. The entire calculation (going from $M = 0$ to $M \simeq 1$) is repeated for different values of ν . A typical traveling wave profile ($M = 0.33$) for small viscosity ($\nu = 0.005$) is shown in Fig. 9(c). The kinetic relation converges to the solid line shown in Fig. 4, which is identical to that derived from inviscid dynamics simulations earlier. We speculate that the numerical damping inherent in our time marching discretization picks the limiting (rather than the exact) inviscid solutions in our dynamic simulations.

The numerical computations above suggest that the inviscid limit is discontinuous: the limit of the viscous solutions as $\nu \rightarrow 0$ differs nontrivially from the solution obtained by setting $\nu = 0$. We speculate briefly on the physical origins of this difference. Recall that when the viscosity is zero, the traveling wave consists of strain oscillations in all space in the traveling frame. These oscillations imply a velocity difference between every pair of points. Thus, the addition of even a small ν would lead to infinitely large dissipation and consequently an infinitely large driving force to sustain this structure. Therefore, one would expect that the oscillations to decay with the slightest addition of viscosity thereby leading to a very different solution.

We now examine this discontinuous limit mathematically. Let $u_0(y)$ be the inviscid solution, and $u(y)$ be the solution with viscosity. These solutions satisfy the equations

$$F(u_0) - M^2 \left(\frac{d^2 u_0(y)}{dy^2} \right) = 0, \tag{6.5a}$$

$$F(u) - \nu M \int \left(\frac{du(y')}{dy'} - \frac{du(y)}{dy} \right) e^{-(y'-y)^2} dy' - M^2 \left(\frac{d^2 u(y)}{dy^2} \right) = 0, \tag{6.5b}$$

where $F(\cdot)$ represents the nonlinear functional containing the elastic peridynamic interactions. We subtract the equations and linearize $F(u)$ about the inviscid solution to obtain

$$T_{u_0} U(y) = \nu M \int \left(\frac{du(y')}{dy'} - \frac{du(y)}{dy} \right) e^{-(y'-y)^2} dy', \tag{6.6}$$

where $U(y) := u(y) - u_0(y)$ and

$$T_{u_0} U(y) := \int_{\mathbb{R}} K(y, y') (U(y') - U(y)) e^{-(y'-y)^2} dy' - M^2 \left(\frac{d^2 U(y)}{dy^2} \right) \tag{6.7}$$

and $K(y, y')$ is the indicator function that is +1 when it connects a stable spring, and -1 when it connects an unstable spring.

As $\nu \rightarrow 0$, the right hand side of (6.6) approaches zero. This would imply that U approaches zero if the spectrum of T_{u_0} is bounded away from zero. If, however, zero is either in the spectrum or an accumulation point of the spectrum of T_{u_0} , then (6.6) is ill-posed and one can have nontrivial solutions for U (see for example, [Engl et al., 2000](#)). We shall now show that we are in the latter situation.

To understand the spectrum of T_{u_0} , we have to first characterize $K(y, y')$. This can be quite complicated as we discussed in the previous section depending on the state about which we linearize. Note that if $K(y, y') = -1$ (respectively, $K(y, y') = +1$) everywhere, then the spectrum is given by $-\pi^{1/2}(1 - e^{-k^2/4}) + M^2 k^2$ (respectively, $\pi^{1/2}(1 - e^{-k^2/4}) + M^2 k^2$). Clearly, 0 is an accumulation point of the spectrum in both these cases.

To study the general case, we verify that the operator T_{u_0} is self-adjoint and thus the spectrum is bounded from above and below by the minimum and maximum values of

$$\begin{aligned} &\langle U(y), T_{u_0} U(y) \rangle \\ &= \frac{1}{2} \int_{\mathbb{R}^2} K(y, y') (U(y') - U(y))^2 e^{-(y'-y)^2} dy' dy - M^2 \int_{\mathbb{R}} \left(\frac{d^2 U(y)}{dy^2} \right) U(y) dy \\ &= \frac{1}{2} \int_{\mathbb{R}^2} (U(y') - U(y))^2 e^{-(y'-y)^2} dy' dy - M^2 \int_{\mathbb{R}} \left(\frac{d^2 U(y)}{dy^2} \right) U(y) dy \\ &\quad - \frac{1}{2} \int_{\mathbb{R}^2} (1 - K(y, y')) (U(y') - U(y))^2 e^{-(y'-y)^2} dy' dy \\ &= -\frac{1}{2} \int_{\mathbb{R}^2} (U(y') - U(y))^2 e^{-(y'-y)^2} dy' dy - M^2 \int_{\mathbb{R}} \left(\frac{d^2 U(y)}{dy^2} \right) U(y) dy \\ &\quad + \frac{1}{2} \int_{\mathbb{R}^2} (1 + K(y, y')) (U(y') - U(y))^2 e^{-(y'-y)^2} dy' dy \end{aligned} \tag{6.8}$$

over all appropriately normalized U , where $\langle \cdot, \cdot \rangle$ denotes the inner product and we have used (A.2). The integrals above containing the terms $1 - K(y, y')$ and $1 + K(y, y')$ are always positive. The remaining terms correspond to the cases considered above, where $K = 1$ or $K = -1$ everywhere. It follows then that 0 is either an accumulation point of the spectrum or is contained in the spectrum for any spatial variation of $K(y, y')$.

7. Interaction of a phase boundary with an inclusion in two dimensions

In this section, we study the problem of a phase boundary, separating two variants of martensite, impinging on an isolated elastic (non-transforming) defect in two dimensions.

We model a material undergoing a square to rectangle phase transformation in two dimensions by using an energy that has two minima that are related by square symmetry. As shown schematically in Fig. 10(a), we use trilinear springs in the $\mathbf{e}_1 = \begin{pmatrix} 1 \\ 0 \end{pmatrix}$ and $\mathbf{e}_2 = \begin{pmatrix} 0 \\ 1 \end{pmatrix}$ directions and we add linear springs in the $(\mathbf{e}_1 + \mathbf{e}_2)/\sqrt{2}$ direction to prevent both springs simultaneously being in the low- or high-strain phase. We smoothen the angular dependence by multiplying by a sinusoidal function. Putting all these together, we arrive at the following constitutive relation:

$$\mathbf{f}(\delta\mathbf{u}, \delta\mathbf{x}) = (f_2(\lambda)\cos^2(2\phi) + f_1(\lambda)\sin^2(2\phi)) \frac{\delta\mathbf{x} + \delta\mathbf{u}}{|\delta\mathbf{x} + \delta\mathbf{u}|} e^{-|\delta\mathbf{x}|^2}, \tag{7.1}$$

where $\lambda := (|\delta\mathbf{x} + \delta\mathbf{u}|/|\delta\mathbf{x}|) - 1$, $\tan \phi := \delta x_2/\delta x_1$ and the functions f_1, f_2 are the one-well and two-well springs:

$$f_1 = 2\lambda, \tag{7.2a}$$

$$f_2 = \begin{cases} \lambda - 0.1 & \text{if } \lambda > 0.05, \\ -\lambda & \text{if } -0.05 < \lambda < 0.05, \\ \lambda + 0.1 & \text{if } \lambda < -0.05. \end{cases} \tag{7.2b}$$

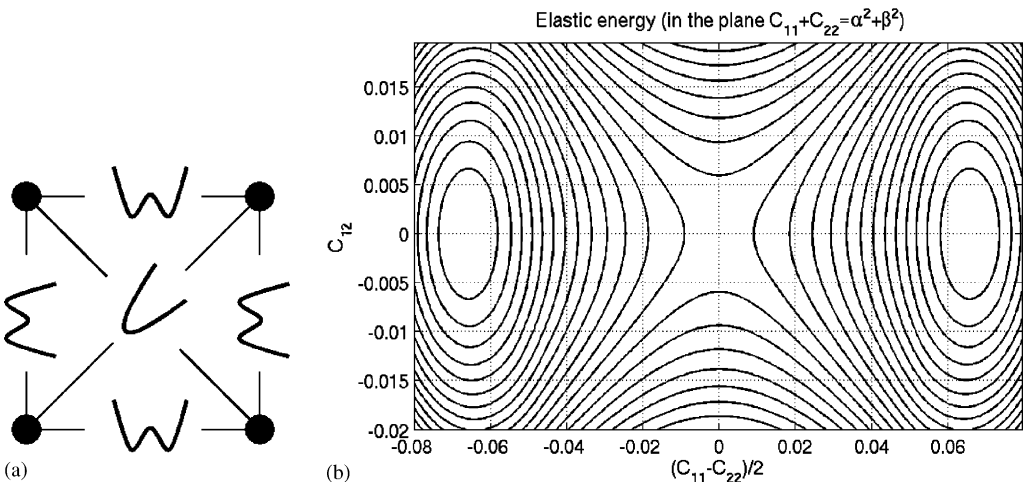


Fig. 10. Model of a two-well material in peridynamics. (a) The unit cell consists of one- and two-well springs. (b) The level sets of the energy density show two wells: (a) unit cell and (b) energy density.

Fig. 10(b) shows the level sets of the macroscopic energy density when the material is subjected to a homogeneous deformation $\mathbf{y} = \mathbf{F}\mathbf{x}$. It is plotted as a function of $C_{11} - C_{22}$ and C_{12} with $C_{11} + C_{22}$ held fixed, where $\mathbf{C} = \mathbf{F}^T\mathbf{F}$. The energy has two wells at

$$\mathbf{U}_1 = \begin{pmatrix} \alpha & 0 \\ 0 & \beta \end{pmatrix}, \quad \mathbf{U}_2 = \begin{pmatrix} \beta & 0 \\ 0 & \alpha \end{pmatrix}, \tag{7.3}$$

where $\alpha = 1 + 0.0645$, $\beta = 1 - 0.0730$ for the particular choice of parameters.

The inclusion is modeled after a nontransforming elastic material. Therefore the constitutive relation in this region is chosen to be

$$\mathbf{f}(\delta\mathbf{u}, \delta\mathbf{x}) = (\lambda \cos^2(2\phi) + 2\lambda \sin^2(2\phi)) \frac{\delta\mathbf{x} + \delta\mathbf{u}}{|\delta\mathbf{x} + \delta\mathbf{u}|} e^{-|\delta\mathbf{x}|^2}, \tag{7.4}$$

where ϕ, λ are as defined earlier. The macroscopic energy density of this material has a single well at the identity. We also choose this same constitutive relation for springs connecting pairs of points that have one point in the inclusion and the other in the martensite.

We recall from the classical theory of martensites (see for example, Bhattacharya, 2003) that two wells with transformation matrices given by (7.3) are in fact compatible, i.e., we can find a rotation matrix \mathbf{Q} and vectors $\mathbf{a}, \hat{\mathbf{n}}$ such that

$$\mathbf{Q}\mathbf{U}_2 - \mathbf{U}_1 = \mathbf{a} \otimes \hat{\mathbf{n}}, \tag{7.5}$$

and thus a material with these wells can form phase (or twin) boundaries with normal $\hat{\mathbf{n}}$ in the reference configuration. For the matrices given by (7.3), $\hat{\mathbf{n}} = (\mathbf{e}_1 \pm \mathbf{e}_2)/\sqrt{2}$. For this reason, it is convenient to work in an orthonormal coordinate system aligned with the twin boundaries, $\mathbf{e}_x = (\mathbf{e}_1 + \mathbf{e}_2)/\sqrt{2}$ and $\mathbf{e}_y = (\mathbf{e}_1 - \mathbf{e}_2)/\sqrt{2}$.

We seek to study the propagation of a phase boundary and its interaction with a nontransforming precipitate. Therefore we consider a rectangular region marked in Fig. 11 with a dashed line as the domain of interest. We use periodic boundary conditions in the y direction. We seek to simulate infinite length in the x direction with fixed far field strain. Therefore we pad the domain of interest with dissipative buffer regions to prevent reflection of acoustic waves and clamp the far ends. Preventing reflection through the use of dissipative boundary layers increases the length of time that the system can be evolved to get usable results. The dissipation is linear in the velocity difference as in the

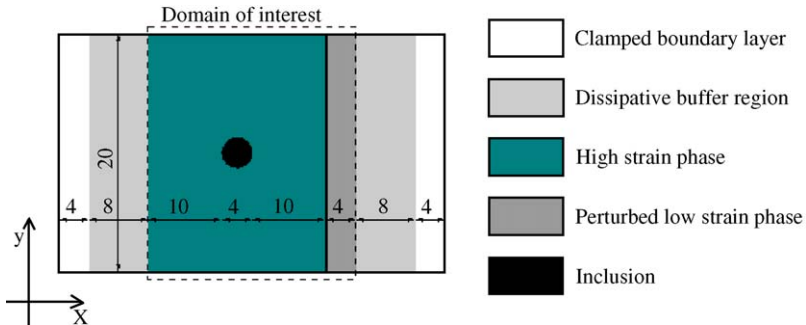


Fig. 11. Initial and boundary conditions for the two-dimensional dynamic calculation.

one-dimensional calculation, and the coefficient of viscous damping is gradually increased in the dissipative regions, as a sudden change in material properties would cause reflections at the interface of the damped and undamped regions.

We study a problem similar to the release problem in Section 4. We place a single phase boundary as shown in Fig. 11 and equilibrate the system. The equilibrium state has significant residual stress because of the nontransforming inclusion since its energy well is different from either of the phases and the circular boundary has both compatible and incompatible directions. The residual stress dies out quickly away from the inclusion and is not significant at the initial phase boundary. We now perturb the martensite on the right side of the phase boundary, by changing the displacement gradient $F_{i1} \mapsto (1 + \varepsilon)F_{i1}$. This perturbation maintains the continuity of the displacement field in the y -direction. Also, as the perturbation is uniform in the y -direction, the driving force is constant at all points along the phase boundary and the phase boundary remains straight until it interacts with the stress field caused by the inclusion. With these initial and boundary conditions, we integrate the peridynamic equation of motion (2.1) in time and examine the evolution of the displacement fields.

The mechanism that the phase boundary uses to move past the inclusion is interesting. Fig. 12 shows snapshots of the deformation field⁴ C_{22} at different times. The phases can be easily differentiated on the basis of high and low values of C_{22} . The inclusion is the prominent circular region in the center of the viewing area with a moderate value of C_{22} . As the phase boundary begins to move toward the inclusion, it also sends off acoustic waves that go ahead of it. When these acoustic waves hit the inclusion, they interact with the stress field and nucleate phase boundaries there that lead to a region of the low-strain phase in the neighborhood of the inclusion. This low-strain region near the inclusion then grows toward the left and consumes the high-strain region beyond. The original phase boundary stops some distance away leaving a remnant of untransformed high-strain martensite partially surrounding the inclusion.

The mechanics of the two-dimensional problem involve a balance between the energy that the phase boundary would require to deviate from the compatible direction imposed by the crystalline basis and the elastic energy that would be required for the large distortions were the phase boundary to move past the inclusion while remaining straight. The single variant of martensite is not compatible with the inclusion and the acoustic wave provides enough energy for microstructure to begin nucleating that then grows and takes energy away from the original phase boundary.

There is experimental evidence of such a mechanism, in micrographs that show the long slivers that are remnants of untransformed material near inclusions (James, 2005).

We have repeated these calculations with smaller and larger driving force. With very small driving force the acoustic wave passes through the inclusion with no nucleation. The original phase boundary gradually slows down and eventually comes to rest before reaching the inclusion. With a large driving force across the phase boundary, we find that the motion of the phase boundary is relatively unaffected by the presence of the inclusion in its movement across the domain, and it causes large deformations in the inclusion as it sweeps over it (Fig. 13). Some acoustic waves are reflected back due to the presence of the inclusion, as can be seen in the figure.

⁴While all calculations in the peridynamic theory involve only the displacement field and not its derivatives, we calculate C as a post-processing step to aid visualization of the results.

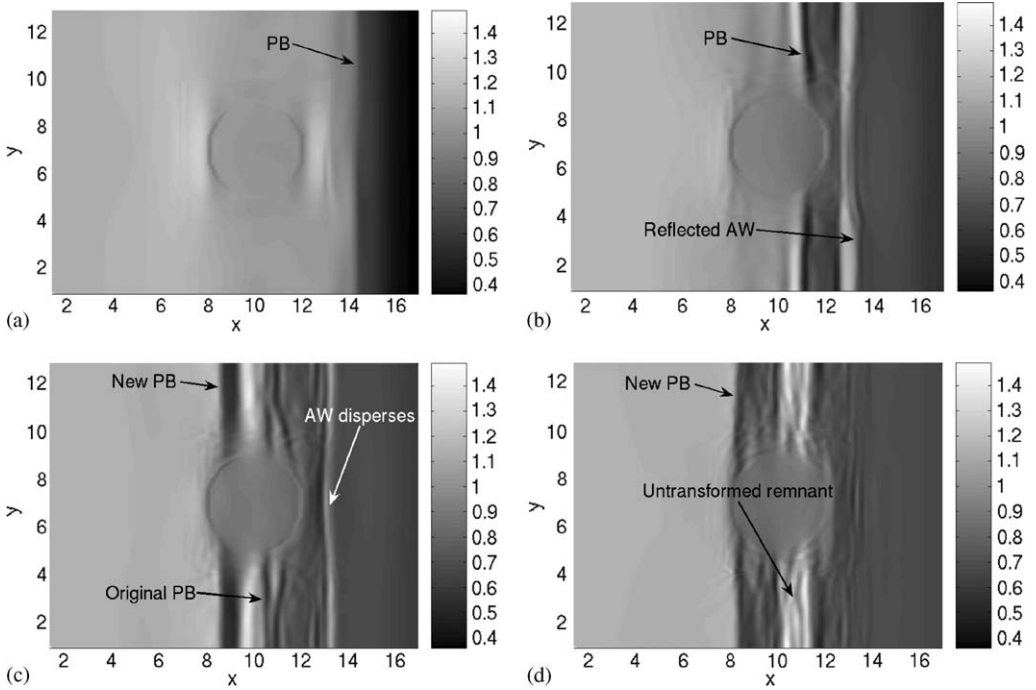


Fig. 12. Interaction of the phase boundary with the inclusion at moderate velocities visualized through a plot of C_{22} . We have used PB to label phase boundaries, and AW to label acoustic waves: (a) phase boundary approaching the inclusion; (b) phase boundary hitting inclusion and acoustic wave reflected; (c) new phase boundary nucleates and original phase boundary stops, while acoustic wave disperses and (d) nucleated phase boundary continues moving leaving behind remnant of untransformed martensite.

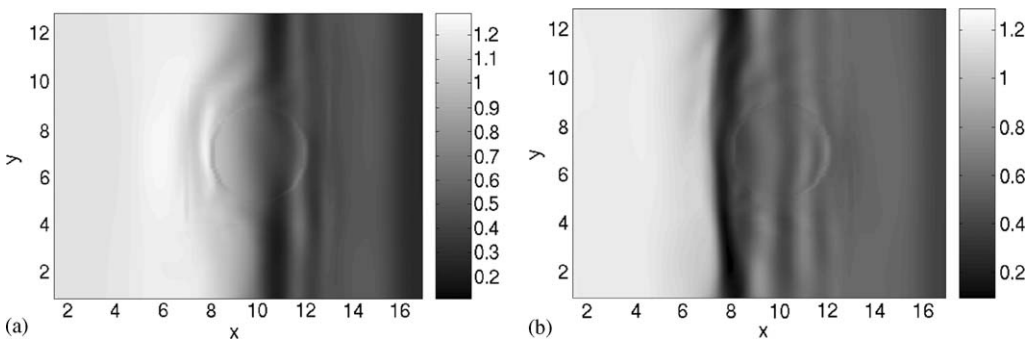


Fig. 13. Interaction of the phase boundary with the inclusion at large velocities visualized through a plot of C_{22} . (a) Phase boundary moving over the inclusion and (b) phase boundary moving past the inclusion.

The results above do not depend strongly on the orientation of the anisotropy in the inclusion. We have repeated the calculations with the anisotropy rotated by angles of $\pi/4$ and $\pi/8$ and we got similar results. The rotation of the anisotropy corresponds to the inclusion having different orientations of the crystalline lattice.

8. Discussion

In this paper we have examined the kinetics of phase transformations in the peridynamic formulation of continuum mechanics. We find that phase boundaries nucleate and propagate naturally and uniquely in this theory. We only need to specify the inter-particle interaction law and do not need to specify any additional conditions like the nucleation criterion or the kinetic relation. Further, we characterize the conditions under which nucleation occurs and the kinetic relations that govern the propagation of a phase boundary. Furthermore, we find that topology transitions occur easily and naturally. Finally, numerical simulations are easy to implement since they involve no spatial derivatives. For all these reasons, we conclude that peridynamics is a very attractive theory for computational studies of martensitic phase transformations.

It is common practice in the literature to study quasistatic hysteresis using a sequence of incremental loading followed by equilibration as we did in Section 3. Our results, in particular our analysis of nucleation, shows that this can depend very much on the numerical method and the size of the incremental load step. Therefore one should be cautious in interpreting the results of such computations.

We have studied nucleation viewing it as a dynamic instability. It provides a criterion that is consistent with our numerical studies. Our viewpoint is different from the classical energetic view of nucleation. It also differs from the viewpoint of [Abeyaratne and Knowles \(1991b\)](#) based on thermodynamic driving force. In the latter two views, one examines whether a perturbation that introduces a second phase grows, while we examine the dynamic stability of a slightly perturbed single phase solution (it is not necessary for the perturbation to be large enough to include the other stable phase). Therefore, a relation between our viewpoint and the others is unclear. As peridynamics is able to resolve the structure of the interface rather than treating it as a sharp discontinuity, we speculate that our analysis may be considered microscopic as opposed to the alternate viewpoints. This distinction places the usual regularized theories on the microscopic side, and hence this criterion may hold in those theories as well.

We have revisited the regularized continuum theory with strain gradients and viscosity and studied nucleation from the viewpoint of dynamic stability in Appendix B. We have found an important difference between that theory and peridynamics. In the regularized continuum theory, the defect size depends only on the size of the region in the unstable phase and not on the difference between the ambient strain and the unstable strain. This reflects the local nature of this theory. In contrast, in peridynamics which is a nonlocal theory, the defect size depends on both the size of the region in the unstable phase and on the difference between the ambient strain and the unstable strain. This has important consequences. Suppose we introduce a large perturbation in a small region of space. Whether this leads to a nucleation is independent of ambient strain in the regularized theory, but significantly dependent in the peridynamic theory. Consequently, if the spatial extent of this perturbation is small enough, it will not lead to nucleation in the regularized theory no matter how close the ambient strain is to the unstable phase, but will do so in the peridynamic formulation. We believe that this is the reason why nucleation has been found to be extremely difficult in computational studies of the regularized and phase-field theories and various researchers have had to resort to noise, pre-nuclei and low-barrier regions. In contrast, the calculations in this paper show that nucleation is relatively simple in this formulation.

Our calculations show that phase boundaries may be viewed as traveling waves. These traveling waves have leading and trailing oscillations that decay as we move away from the phase boundary. The rate of decay depends on viscosity, but the wavelength is relatively independent. The velocity of the traveling wave depends on the average far field conditions only through a driving force, so that this analysis leads to a kinetic relation. The kinetic relation with viscosity leads to large dissipation for small speeds, but curiously smaller dissipation for larger phase boundary velocities, compared to the inviscid case. We do not understand this curious cross-over, but note that a similar result has been found in regularized theories (Abeyaratne and Knowles, 1991a). The kinetic relation goes continuously through the origin (i.e., the velocity and the driving force approach zero together). There is also a limiting velocity which is the sound speed of both phases (these are assumed equal and constant in the trilinear material). We have also carried out similar calculations for a material with a cubic polynomial stress response function. The kinetic relation with viscosity does not have a limiting velocity, and this is not surprising since the high-strain phase has unbounded sound speed.

While small amplitude waves in either of the stable phases of our peridynamic material are dispersive, it is interesting that we find traveling wave structures that involve all phases. Like other solitons, we believe that the nonlinearity and the dispersion balance each other for special structures and allow them to be traveling waves.

We close by pointing out two interesting and open problems. We have shown that nucleation and kinetics arise from a specification of a force field in the peridynamic formulation. However, the range of nucleation conditions and kinetic relations that can be obtained from within the peridynamic formulation remains unknown. Similarly, it remains unclear whether one can alter the kinetic and static properties independently. Finally, an examination of nucleation from the point of view of dynamic instability in higher dimensions and also in atomistic systems would be very interesting.

Acknowledgments

We thank Stewart Silling, Mathias Jungen, James Knowles, Markus Zimmermann, and Rohan Abeyaratne for useful discussions. We are grateful for the financial support of the Sandia National Labs and the National Science Foundation.

Appendix A. Bounds on the spectrum of a non-ideal defect

We derive here bounds on the spectrum of a non-ideal defect, using the results that we have for an ideal defect. We recall that a non-ideal defect has a nontrivial mixed region as described in Fig. 7(b). For such a defect, with a given δ^u and δ^l , we expect that an ideal defect of size δ will be more stable than a non-ideal defect when $\delta^l = \delta$, as the non-ideal defect would have as large an inner unstable region as the ideal defect, as well as more unstable springs outside this inner region, while the ideal defect would have no unstable springs outside the inner region. Similarly, we expect that an ideal defect of size δ will be less stable than a non-ideal defect when $\delta^u = \delta$, as the non-ideal defect would have some stable springs in the inner region while the ideal defect would have only unstable springs in the inner region. We make these bounds rigorous by means of standard inequalities that

are well-known

$$\int_{\Omega} f(x)g(x) \, dx \leq \left(\int_{\Omega} f(x)^2 \, dx \right)^{1/2} \left(\int_{\Omega} g(x)^2 \, dx \right)^{1/2}, \tag{A.1a}$$

$$\int_{\Omega} |f(x) + g(x)|^2 \, dx \leq \left(\left(\int_{\Omega} f(x)^2 \, dx \right)^{1/2} + \left(\int_{\Omega} g(x)^2 \, dx \right)^{1/2} \right)^2, \tag{A.1b}$$

$$\int_{\Omega} |f(x)||g(x)| \, dx \leq |f(x)|_{\max} \int_{\Omega} |g(x)| \, dx \tag{A.1c}$$

for $f(x), g(x) \in L_2(\Omega)$.

For a non-ideal defect with radii δ^u and δ^l , where $\delta^u = \delta$, we write the inner product

$$\begin{aligned} I_{\delta^u}(v) &= \int_{\mathbb{R}^2 - (-\delta, \delta)^2} e^{-(x'-x)^2} (v(x)^2 - v(x)v(x')) \, dx \, dx' \\ &\quad + \int_{(-\delta, \delta)^2} K(x, x') e^{-(x'-x)^2} (v(x)^2 - v(x)v(x')) \, dx \, dx' \\ &= \int_{\mathbb{R}^2} e^{-(x'-x)^2} (v(x)^2 - v(x)v(x')) \, dx \, dx' \\ &\quad - 2 \int_{(-\delta, \delta)^2} e^{-(x'-x)^2} (v(x)^2 - v(x)v(x')) \, dx \, dx' \\ &\quad + \int_{(-\delta, \delta)^2} (1 + K(x, x')) e^{-(x'-x)^2} (v(x)^2 - v(x)v(x')) \, dx \, dx' \\ &= I_{\delta}(v) + \int_{(-\delta, \delta)^2} (1 + K(x, x')) e^{-(x'-x)^2} (v(x)^2 - v(x)v(x')) \, dx \, dx', \end{aligned}$$

where $K(x, x')$ is an indicator function that is -1 when x, x' are connected by an unstable spring, and $+1$ when they are connected by a stable spring. The second term in the final form above indicates the difference between the inner product of a non-ideal defect and that of an ideal defect.

We normalize $v(x)$ by setting $v(x)$ to have unit L_2 norm over a finite region larger than δ^u , while retaining the restriction that $v(x)$ is such that the integrals appearing in the inner product are bounded.

Since $K(x, x')$ is symmetric in its arguments, we can exchange x, x' in the second term and add the result to the original integral to arrive at

$$\begin{aligned} &\int_{(-\delta, \delta)^2} (1 + K(x, x')) e^{-(x'-x)^2} (v(x)^2 - v(x)v(x')) \, dx \, dx' \\ &= \frac{1}{2} \int_{(-\delta, \delta)^2} (1 + K(x, x')) e^{-(x'-x)^2} (v(x) - v(x'))^2 \, dx \, dx', \end{aligned} \tag{A.2}$$

where the integrand is non-negative everywhere on the domain of integration and hence this term is bounded below by 0. For an upper bound on this term

$$\begin{aligned}
 & \frac{1}{2} \int_{(-\delta, \delta)^2} (1 + K(x, x')) e^{-(x'-x)^2} (v(x) - v(x'))^2 \, dx \, dx' \\
 & \leq \int_{(-\delta, \delta)^2} (v(x) - v(x'))^2 \, dx \, dx' \\
 & \leq \int_{(-\delta, \delta)} \left(\left(\int_{(-\delta, \delta)} v(x)^2 \, dx \right)^{1/2} + \left(\int_{(-\delta, \delta)} v(x')^2 \, dx' \right)^{1/2} \right)^2 \, dx \\
 & \leq \int_{(-\delta, \delta)} (v(x)(2\delta^u)^{1/2} + 1)^2 \, dx \\
 & \leq \int_{(-\delta, \delta)} v(x)^2 (2\delta^u) \, dx + \int_{(-\delta, \delta)} 1 \, dx + 2 \int_{(-\delta, \delta)} v(x)(2\delta^u)^{1/2} \, dx \\
 & \leq 8\delta^u,
 \end{aligned}$$

where we have used inequality (A.1c) to go to the second step, inequality (A.1b) to go to the third step, the normalization of $v(x)$ to bound the second term and go the fourth step, expanded the square to reach the fifth step, used again the normalization of $v(x)$ to bound the first term and inequality (A.1a) to bound the third term as follows:

$$\int_{(-\delta, \delta)} v(x)(2\delta^u)^{1/2} \, dx \leq \left(\int_{(-\delta, \delta)} v(x)^2 \, dx \right)^{1/2} \left(\int_{(-\delta, \delta)} (2\delta^u) \, dx \right)^{1/2}$$

and using again the normalization of $v(x)$.

We also see that the integrand in the above expression is 0 in the interior of the square $(-\delta^1, \delta^1)^2$ and hence has no contribution, and the integral in this region can be bounded above by $8\delta^1$ in the same manner as for the integral over the square $(-\delta, \delta)^2$. So, we can now write the upper and lower bounds as

$$0 \leq \frac{1}{2} \int_{(-\delta, \delta)^2} (1 + K(x, x')) e^{-(x'-x)^2} (v(x) - v(x'))^2 \, dx \, dx' \leq 8(\delta^u - \delta^1).$$

We now turn to the case when the non-ideal defect has $\delta^1 = \delta$. Writing the inner product

$$\begin{aligned}
 I_{\delta^1}(v) &= \int_{\mathbb{R}^2 - (-\delta^u, \delta^u)^2} e^{-(x'-x)^2} (v(x)^2 - v(x)v(x')) \, dx \, dx' \\
 &\quad - \int_{(-\delta, \delta)^2} e^{-(x'-x)^2} (v(x)^2 - v(x)v(x')) \, dx \, dx' \\
 &\quad + \int_{(-\delta^u, \delta^u)^2 - (-\delta, \delta)^2} K(x, x') e^{-(x'-x)^2} (v(x)^2 - v(x)v(x')) \, dx \, dx' \\
 &= \int_{\mathbb{R}^2} e^{-(x'-x)^2} (v(x)^2 - v(x)v(x')) \, dx \, dx' \\
 &\quad - 2 \int_{(-\delta, \delta)^2} e^{-(x'-x)^2} (v(x)^2 - v(x)v(x')) \, dx \, dx'
 \end{aligned}$$

$$\begin{aligned}
 & - \int_{(-\delta^u, \delta^u)^2 - (-\delta, \delta)^2} (1 - K(x, x')) e^{-(x'-x)^2} (v(x)^2 - v(x)v(x')) \, dx \, dx' \\
 = & I_\delta(v) - \int_{(-\delta^u, \delta^u)^2 - (-\delta, \delta)^2} (1 - K(x, x')) e^{-(x'-x)^2} (v(x)^2 - v(x)v(x')) \, dx \, dx'.
 \end{aligned}$$

We can bound the difference between inner products following the same steps as for the previous bound with the appropriate modifications to arrive at the analogous bounds.

We summarize the results of these bounds as

$$I_\delta(v) \leq I_{\delta^u}(v) \leq I_\delta(v) + 8(\delta^u - \delta^1) \quad \text{when } \delta^u = \delta, \tag{A.3a}$$

$$I_\delta(v) - 8(\delta^u - \delta^1) \leq I_{\delta^1}(v) \leq I_\delta(v) \quad \text{when } \delta^1 = \delta \tag{A.3b}$$

for a given $v(x)$. We can immediately see from these bounds that if $\text{erf}(\delta^u) < \frac{1}{2}$, the non-ideal defect must be stable, and if $\text{erf}(\delta^1) > \frac{1}{2}$, the non-ideal defect must be unstable.

Appendix B. Nucleation in a regularized theory

We study nucleation in a classical continuum theory augmented with viscosity and strain gradient (Abeyaratne and Knowles, 1991a). We use their model here without the viscous dissipation:

$$\rho \partial_{tt} u(x, t) = \partial_x (\hat{\sigma}(\partial_x u(x, t))) - \rho \lambda \partial_{xxxx} u(x, t), \tag{B.1}$$

where λ is the coefficient of surface energy and $\hat{\sigma}(\cdot)$ is the non-monotone stress response function.

Following the procedure that we used to study the peridynamic theory, we assume that a low-strain field evolves and leads to a region of unstable strain. We then linearize the equations around this state and test the stability as a function of the defect size. For simplicity, we use a stress-response function that is bilinear and with equal and opposite slopes $\pm E_0$ ($E_0 > 0$) on the branches. Adding a small perturbation $\varepsilon v(x, t)$ to the displacement field $u(x, t)$ and differentiating the resulting equation with respect to ε leads to the linearized equation in $v(x, t)$

$$\rho \partial_{tt} v(x, t) = \partial_x (E(x) \partial_x v(x, t)) - \rho \lambda \partial_{xxxx} v(x, t), \tag{B.2}$$

where $E(x) = \hat{\sigma}'(u(x, t)) = \pm E_0$ is the slope of the stress response and switches between stable and unstable as a function of position, $E(x) = -E_0$ for $|x| < \delta$ and $E(x) = E_0$ elsewhere.

Decomposing $v(x, t) = v(x) e^{i\omega t}$ into sinusoidal modes and taking the inner product $I_\delta^{\text{sg}} = \langle v(x), L_\delta^{\text{sg}} v(x) \rangle$ gives

$$I_\delta^{\text{sg}}(v) = \int_{\mathbb{R}} \rho \lambda v(x) v^{(4)}(x) \, dx - \int_{\mathbb{R}} E_0 v(x) v^{(2)}(x) \, dx + \int_{(-\delta, \delta)} 2E_0 v(x) v^{(2)}(x) \, dx,$$

where the inner product is defined as in peridynamics.

Taking the limit of $\delta = 0$ and using the decomposition $v_k(x) = e^{ikx}$ allows us to calculate the spectrum $\rho \lambda k^4 + E_0 k^2$ which is stable for $k > 0$.

Taking the limit of $\delta \rightarrow \infty$ and using the decomposition $v_k(x) = e^{ikx}$, we find the spectrum is $\rho \lambda k^4 - E_0 k^2$ which is unstable for $k < 1/\gamma$, where $\gamma := \sqrt{\rho \lambda / E_0}$ is the lengthscale associated with the strain gradient model. The strain gradient theory differs

from the peridynamic theory in that the surface energy contribution has a stabilizing effect in both the stable and unstable regions, whereas in peridynamics the entire energy changes sign in the unstable regions.

It is straightforward to show that the operator is unstable at finite δ by using a test function that is localized within the defect. To show that the operator is stable for finite δ , we use integration by parts to rewrite the surface energy contribution, and rescale $v(x) = \tilde{v}(x/\delta) = \tilde{v}(y)$. This gives

$$I_{\delta}^{\text{sg}}(v) = \frac{1}{\delta^2 E} \left(\left(\frac{\gamma}{\delta} \right)^2 \int_{\mathbb{R}} (\tilde{v}^{(2)}(y))^2 dy - \int_{\mathbb{R}} \tilde{v}(y) \tilde{v}^{(2)}(y) dy + \int_{(-1,1)} 2\tilde{v}(y) \tilde{v}^{(2)}(y) dy \right).$$

From the continuity and jump requirements on $v(x, t)$ and its derivatives (Abeyaratne and Knowles, 1991a), the first integral in the expression above is positive and finite, and the remaining integrals are finite. So, for any $\tilde{v}(y)$, we can always find a value of $\delta > 0$ that makes the first positive integral sufficiently large that the entire expression is positive. The form of the expression above also shows that the critical defect size scales with the internal length scale of the material γ prescribed by the choice of surface energy coefficient.

This calculation highlights an important difference between the nonlocal peridynamic theory and strain gradient theories. In the peridynamic theory, the formation of a small area of unstable phase that is surrounded by a stable region of low-strain phase that is close to the peak strain has a large effective defect size due to the fact that many of the surrounding springs are easily stretched beyond the peak strain. Similarly, a defect surrounded by low-strain phase that is well below the peak strain has a smaller effective size. This dependence of the effective defect size on the strain in the neighborhood is unique to peridynamics. The ability of peridynamics to capture the effect of the surroundings makes it very different from a strain gradient theory in this respect.

References

- Abeyaratne, R., Knowles, J.K., 1990. On the driving traction on a surface of a strain discontinuity in a continuum. *J. Mech. Phys. Solids* 38, 345–360.
- Abeyaratne, R., Knowles, J.K., 1991a. Implications of viscosity and strain gradient effects for the kinetics of propagating phase boundaries in solids. *SIAM J. Appl. Math.* 51 (5), 1205–1221.
- Abeyaratne, R., Knowles, J.K., 1991b. Kinetic relations and the propagation of phase boundaries in solids. *Arch. Ration. Mech. Anal.* 114, 119–154.
- Anderson, E., Bai, Z., Bischof, C., Blackford, S.L., Demmel, J.W., Dongarra, J.J., DuCroz, J., Greenbaum, A., Hammarling, S., McKenney, A., Sorensen, D., 1999. *LAPACK User's Guide*, third ed. Society for Industrial and Applied Mathematics.
- Artemev, A., Jin, Y., Khachatryan, A., 2001. Three-dimensional phase field model of proper martensitic transformation. *Acta Mater.* 49 (7), 1165–1177.
- Ball, J.M., James, R.D., 2005. Metastability in martensitic phase transformations. In preparation.
- Bhattacharya, K., 2003. *Microstructure of Martensite*. Oxford University Press, Oxford.
- Christian, J.W., 1975. *The Theory of Transformations in Metals and Alloys*. Pergamon, New York.
- Dondl, P.W., Zimmer, J., 2004. Modeling and simulation of martensitic phase transitions with a triple point. *J. Mech. Phys. Solids* 52 (9), 2057–2077.
- Engl, H.W., Hanke, M., Neubauer, A., 2000. *Regularization of Inverse Problems*. Kluwer Academic Publishers, Dordrecht.
- Eshelby, J.D., 1956. *Solid State Physics*, vol. 3. Academic Press, New York, pp. 17–144.
- Eshelby, J.D., 1975. The elastic energy–momentum tensor. *J. Elasticity* 5, 321–335.
- James, R.D., 2005. Unpublished micrographs.

- Killough, M.G., 1998. A diffuse interface approach to the development of microstructure in martensite. Ph.D. Thesis, New York University.
- Kloucek, P., Luskin, M., 1994. Computational modeling of the martensitic transformation with surface energy. *Math. Comput. Model.* 20, 101–121.
- Kunin, I.A., 1982. Elastic media with microstructure. Springer Series in Solid-State Sciences, vol. 26. Springer, Berlin.
- Lefloch, P., 1993. Propagating phase boundaries: formulation of the problem and existence via the Glimm method. *Arch. Ration. Mech. Anal.* 123, 153–197.
- Lei, Y., Friswell, M.I., Adhikari, S., 2006. A Galerkin method for distributed systems with non-local damping. *Int. J. Solids Struct.* 43, 3381–3400.
- Olson, G.B., Roitburd, A.L., 1992. Martensitic nucleation. In: *Martensite*. ASM, pp. 149–174 (Chapter).
- Porter, D., Stirling, D.G.S., 1990. *Integral Equations*. Cambridge University Press, Cambridge.
- Purohit, P.K., 2001. Dynamics of phase transitions in strings, beams and atomic chains. Ph.D. Thesis, California Institute of Technology.
- Silling, S.A., 2000. Reformulation of elasticity theory for discontinuities and long-range forces. *J. Mech. Phys. Solids* 48, 175–209.
- Silling, S.A., Kahan, S., 2004. Peridynamic modeling of structural damage and failure. In: *Conference on High Speed Computing*, Glendon Beach, Oregon, USA.
- Silling, S.A., Zimmermann, M., Abeyaratne, R., 2003. Deformation of a peridynamic bar. *J. Elasticity* 73, 173–190.
- Truskinovsky, L., 1993. Kinks versus shocks. In: Fosdick, R., Dunn, E., Slemrod, M. (Eds.), *Shock Induced Transitions and Phase Structures in General Media*, IMA, vol. 52. Springer, Berlin.
- Truskinovsky, L., Vainchtein, A., 2005. Kinetics of martensitic phase transitions: lattice model. *SIAM J. Appl. Math.* 66 (2), 533–553.
- Wang, Y.Z., Chen, L.Q., Khachaturyan, A.G., 1994. Computer simulation of microstructure evolution in coherent solids. In: *Solid–Solid Phase Transformations*. The Minerals Metals and Material Society, pp. 245–265 (Chapter).
- Weckner, O., Abeyaratne, R., 2005. The effect of long-range forces on the dynamics of a bar. *J. Mech. Phys. Solids* 53, 705–728.
- Zimmermann, M., 2002. Phase transformations in the one dimensional peridynamic theory. Unpublished private communication.